From crustal thickening to orogen-parallel escape: the 120 Ma-long HT-LP evolution of the Paleozoic Famatinian back-arc, NW Argentina

Pablo Guillermo Farias[1,1], Roberto F. Weinberg[1,1], Alfonso Sola[2,2], and Raúl Becchio[3,3]

[1]Monash University
[2]Universidad de Salta. IBIGEO-CONICET
[3]INENCO-CONICET

November 30, 2022

Abstract

Exposed sections of accretionary orogens allow reconstruction of their tectonic evolution. Most commonly, orogens are characterised by two-dimensional shortening perpendicular to the orogenic front. We describe the mid-crustal section of the back-arc of the early Paleozoic Famatinian accretionary orogen, exposed in the Sierra de Quilmes. Here crustal deformation evolved from a typical two-dimensional shortening with tectonic transport towards the west, to a non-coaxial constrictional strain with a southward tectonic transport parallel to the orogen. During the early phase of deformation, HT-LP metamorphic complexes were juxtaposed by west-directed thrusting on remarkably thick shear zones forming a thrust duplex. Deformation of the buried footwall complex continued after the exhumed hanging wall ceased to deform. We suggest that the thermally-weakened footwall complex responded by initiating a phase of south-verging thrusting, parallel to the orogen, associated with strong constriction, associated with L-tectonites, and sheath folds. This late phase of deformation defines a non-coaxial constrictional regime characterized by simultaneous east-west and vertical shortening and strong north-south, orogen-parallel stretching. Titanite ages and Zr-in-titanite thermometry demonstrate that this back-arc remained above 700 °C for 120 Ma between 500 and 380 Ma. Combined with regional geology, the new data suggest that west-verging thrusting interrupted an early, back-arc extensional phase, and lasted from ˜ 470 to 440 Ma, and that footwall constriction and south-verging thrusting continued for another 40 to 60 Ma. The Famatinian back-arc exposed in Sierra de Quilmes thus is an example of how shortening and orogenic growth in a hot orogen was counterbalanced by lateral flow.

From crustal thickening to orogen-parallel escape: the 120 Ma-long HT-LP evolution of the Paleozoic Famatinian back-arc, NW Argentina

Pablo Farias[1], Roberto F. Weinberg[1], Alfonso Sola[3], Raul Becchio[2,3].

1. School of Earth, Atmosphere and Environment, Monash University, Clayton, Victoria 3800, Australia
2. LaTe Andes, Las Morereas 510, Vaqueros, Salta, Argentina
3. Instituto Geonorte, Universidad Nacional de Salta, INENCO-CONICET, Av. Bolivia 5150, 4400 Salta, Argentina

Keywords: Accretionary orogeny, Famatinian orogen, HT-LP, long-lived orogen, structural geology, titanite geochronology

Key points:

1-Understanding how crustal thickening in the Famatinian back-arc was counterbalanced by a long-lived orogen-parallel stretching event

2-Titanite geochronology and geothermometry suggest that the footwall block remained hot for ~60 Myr longer than the hanging wall

Plain language summary: This paper contributes to the understanding of the structural and thermal evolution of a mountain belt in a tectonic plate margin. Our study case is the Ordovician Famatinian orogen (mountain belt), in NW Argentina. We found that the orogen reacted to both tectonic and gravitational forces by stretching laterally under constriction rather than growing vertically as its foundations were thermally weakened. Geochronology and thermometry from titanite indicate that the core of this orogen was partially molten for ~100 million years, and cooled very slowly. These partially molten rocks undermined the stability of the orogen and ultimately caused its failure and lateral flow.

Abstract

Exposed sections of accretionary orogens allow reconstruction of their tectonic evolution. Most commonly, orogens are characterised by two-dimensional shortening perpendicular to the orogenic front. We describe the mid-crustal section of the back-arc of the early Paleozoic Famatinian accretionary orogen, exposed in the Sierra de Quilmes. Here crustal deformation evolved from a typical two-dimensional shortening with tectonic transport towards the west, to a non-coaxial constrictional strain with a southward tectonic transport parallel to the orogen. During the early phase of deformation, HT-LP metamorphic complexes were juxtaposed by west-directed thrusting on remarkably thick shear zones forming a thrust duplex. Deformation of the buried footwall complex continued after the exhumed hanging wall ceased to deform. We suggest that the thermally-weakened footwall complex responded by initiating a phase of south-verging thrusting, parallel to the orogen, associated with strong constriction, associated with L-tectonites, and sheath folds. This late phase of deformation defines a non-coaxial constrictional regime characterized by simultaneous east-west and vertical shortening and strong north-south, orogen-parallel stretching. Titanite ages and Zr-in-titanite thermometry demonstrate that this back-arc remained above 700 °C for 120 Ma between 500 and 380 Ma. Combined with regional geology, the new data suggest that west-verging thrusting interrupted an early, back-arc extensional phase, and lasted from ~ 470 to 440 Ma, and that footwall constriction and south-verging thrusting continued for another 40 to 60 Ma. The Famatinian back-arc exposed in Sierra de Quilmes thus is an example of how shortening and orogenic growth in a hot orogen was counterbalanced by lateral flow.

1. Introduction

Rocks within orogens move through evolving thermal and structural fields (Jamieson and Beaumont, 2013). Continental back-arcs in accretionary orogens are characterised by long-lasting high-temperature and low-pressure (HT-LP) metamorphism spread along broad zones (Curie and Hyndman, 2006; Wolfram et al., 2019) due to the thinner lithosphere interacting with the asthenosphere (Heuret et al., 2007; Heuret and Lallemand, 2005; Hyndman et al., 2005). This thermally weakened crustal section is susceptible to deformation in response to subduction dynamics (Curie and Hyndman, 2006; Heuret and Lallemand, 2005; Jamieson and Beaumont, 2013) and can record switches between extension and shortening events (Collins, 2002; Lister and Forster, 2009).

Strain in such orogens can be partitioned into pure and simple shear during compression (Braathen et al., 2000; Carreras et al., 2013; Fletcher and Bartley, 1994; Hajná et al., 2012; Malavieille, 1993; Rubio Pascual et al., 2016; Sullivan, 2009; Sullivan and Law, 2007), or extension (Jolivet et al., 2004; Mancktelow and Pavlis, 1994), and sometimes it can be associated with constriction (Jolivet et al., 2004; Sullivan and Law, 2007). More significantly, a number of papers documented tectonic transport directions that deviates from the direction perpendicular to the orogen. For example, (Chardon et al., 2009) reviewed several Precambrian accretionary orogens where sections of the crust flowed parallel to the orogen in response to tectonic shortening. They suggested that this may be analogous to what happens in current, wide hot orogens, like the Cordilleran or Tibetan belts. Numerical modelling of mid-crustal levels led to several scenarios dominated by orogen-parallel flow (Chardon and Jayananda, 2008; Chardon et al., 2011; Parsons et al., 2016).

Here we investigate the mid-crustal section of a continental back-arc, part of the early Paleozoic (pre-Andean) Famatinian orogen in the Sierra de Quilmes, NW Argentina (Fig. 1). This orogeny was a long-lived, wide and hot accretionary orogeny, located in the active margin of Western Gondwana and part of the regional Terra Australis orogen (Cawood, 2005). The Famatinian back-arc is associated with wide shear zones that accommodated convergence (Finch et al., 2015; Finch et al., 2017; Larrovere et al., 2016; Larrovere et al., 2008; Semenov et al., 2019). It records ca. 60 million years of magmatism and HT-LP metamorphism, between ~500 and 440 Ma (Büttner et al., 2005;

Finch et al., 2017; Ortiz et al., 2019; Sola et al., 2013; Sola et al., 2017; Wolfram et al., 2019). We present new structural and geochronology data that yield insights into processes possibly acting today inside ongoing accretionary orogens like the neighbouring central Andes or the North American Cordillera.

Wolfram et al. (2019) determined that the 60 Ma duration of high heat flux in this area possibly occurred as multiple pulses. Weinberg et al. (2018) argued that the Famatinian orogen widened because it was too hot to give rise to a thick crust. Here we focus on the combined questions surrounding the nature of the long-lived high heat flux and the orogenic flow, to understand how the hot back-arc crust responded to continued E-W crustal shortening. This paper starts with a review of the regional geology including the Sierra de Quilmes. This is followed by the methods and a description of the results of several mapping campaigns before detailing the results of titanite U-Pb geochronology and chemistry. We discuss the results in terms of the 3D evolution of the orogen and how it responded to crustal thickening, and use the thermal and temporal constraints provided by titanite to argue that the orogeny remained hot for 120 Ma.

2 Regional Geology

2.1 Famatinian orogeny in the Sierras Pampeanas

The Sierra de Quilmes is part of the Sierras Pampeanas province (Fig. 1), which comprises a number of north-south trending mountain ranges located between 24° and 34°S and 64° and 68°W (Büttner et al., 2005) in the current Andean foreland of west Argentina. These mountains have been part of an accretionary margin developed along West Gondwana during Paleozoic times, as part of the larger Terra Australis orogen (Cawood, 2005; Schwartz et al., 2008). Due to the current flat-slab subduction under the Andes, the Sierras Pampeanas were uplifted exposing different crustal levels (Ramos, 2009). The Sierras Pampeanas are composed almost exclusively of Neoproterozoic to Paleozoic meta-sedimentary and igneous rocks shaped during the Pampean (~540-520 Ma), Famatinian (~500-440 Ma) and Achalian (~390-350 Ma) orogenies. These orogenies were driven by subduction of the proto-Pacific ocean, and each ended after the accretion of a Laurentian-derived terranes (Aceñolaza et al., 2002; Astini, 1998; Escayola et al., 2011; Omarini et al., 1999; Ramos et al., 1998; Ramos et al., 2000; Ramos et al., 1986; Rapela et al., 1998b; Rapela et al., 2015). Thus, the Famatinian orogenic cycle was a subduction-related Andean-type continental orogeny.

The Famatinian orogeny comprised a magmatic arc forming a N-S belt bound to the west by a back-arc, that was extensively migmatized and that today includes the Sierra de Quilmes (Fig. 1). The orogenic cycle initiated at ~505-500 Ma, as indicated by zircon U/Pb ages in peraluminous magmatic rocks of the Famatinian back-arc (Bahlburg et al., 2016; Wolfram et al., 2017). The back-arc was dominated initially by an extensional tectonic regime with the development of marine sedimentary basins between ~485 and 470 Ma (Astini, 2008; Bahlburg and Breitkreuz, 1991; Bahlburg and Hervé, 1997b; Büttner, 2009; Moya, 2015; Rapela et al., 2018). Deformation in the back-arc switched to shortening after ~470 Ma (Weinberg et al., 2018), starting the event known as the Oclóyic phase (Turner, 1975). This event was triggered by the arrival and docking of the Laurentian-derived Precordillera/Cuyania block to the western margin of Gondwana, and marked by regional unconformities formed during the inversion of the basins (Astini and Dávila, 2004; Bahlburg and Hervé, 1997a; Davila et al., 2003; Ramos, 2008; Thomas and Astini, 2003). This phase was characterized by folding and development of several wide thrusts at mid-crustal levels (Finch et al., 2015; Larrovere et al., 2016; Larrovere et al., 2011; Rapela et al., 1998a; Semenov et al., 2019; Semenov and Weinberg, 2017). The Famatinian orogenic cycle is inferred to have finished at around 440-435 Ma when magmatism waned (2009; Bahlburg et al., 2016; Büttner et al., 2005; Mulcahy et al., 2014; Wolfram et al., 2017).

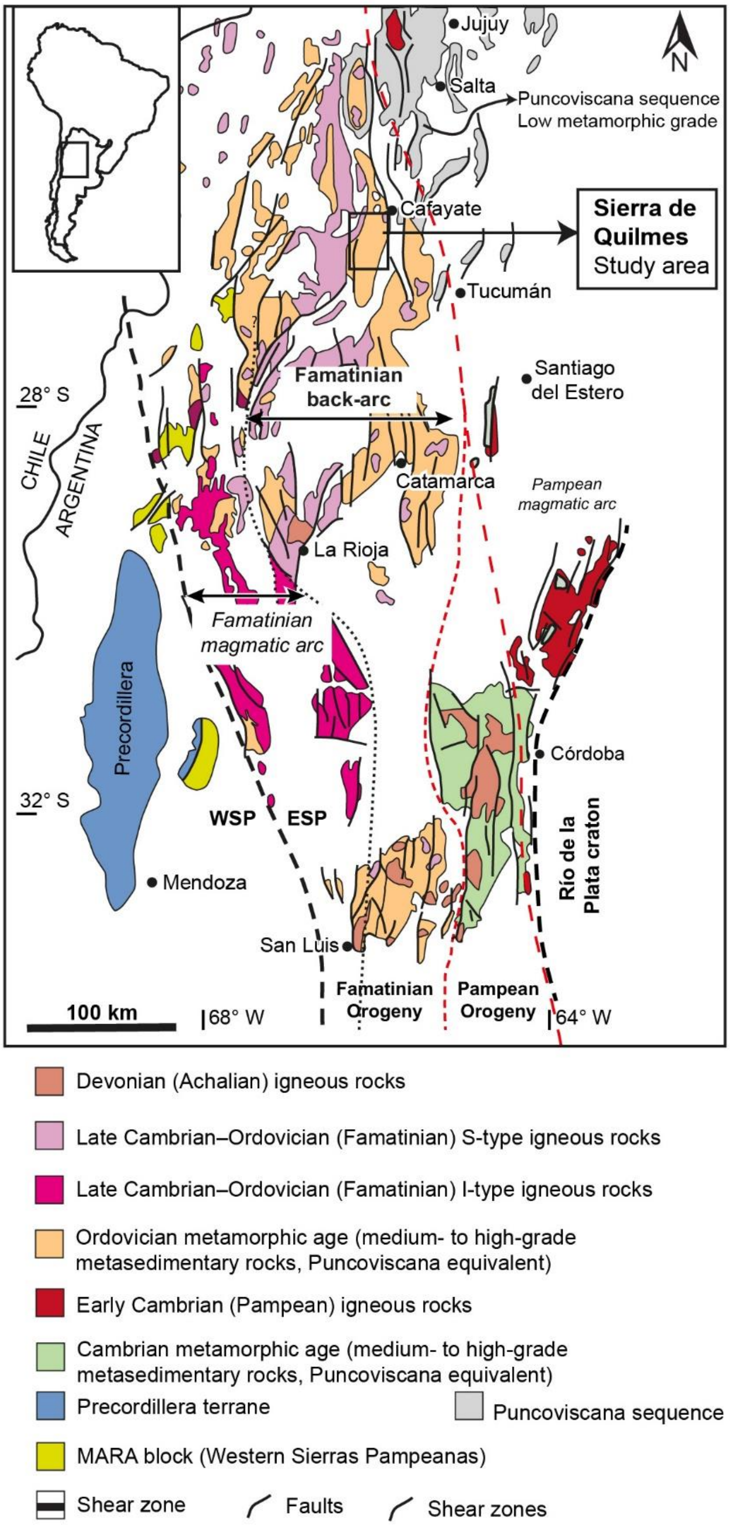

Figure 1. Regional map of Sierras Pampeanas. WSP, Western Sierras Pampeanas (Laurentian-derived terranes), ESP, Eastern Sierras Pampeanas (Gondwana-derived terrane). The Sierra de Quilmes is part of the Famatinian back-arc.

2.2 Geology of the Sierra de Quilmes

The mid-crustal section of the Famatinian back-arc exposed in Sierra de Quilmes comprises dominantly of the Neoproterozoic to Cambrian turbidite of the Puncoviscana sequence (Adams et al., 2011; Rapela, 1976; Toselli et al., 1978). These rocks record HT-LP Buchan series metamorphism, and reached granulite facies undergoing extensive partial melting that gave rise to vast migmatites and peraluminous granite intrusions (Büttner et al., 2005; Finch et al., 2015). Several workers have studied the northern part of the Sierra de Quilmes (Büttner, 2009; Büttner et al., 2005; Finch et al., 2015; Finch et al., 2016; Rossi and Toselli, 1976; Toselli et al., 1978; Wolfram et al., 2017; Wolfram et al., 2019), leaving the southern part of the range relatively unexplored. Toselli et al. (1978) and Rapela (1976) first divided the area into two complexes that record different metamorphic conditions and were juxtaposed tectonically: the Tolombon and the Agua del Sapo complexes (Fig. 2).

2.2.1 Tolombon complex

The Tolombon complex comprises Al-rich siliciclastic turbidites of the Puncoviscana sequence (Toselli et al., 1978). The metamorphic facies in this complex grades over short distances from greenschist facies chlorite zone in the northeast to granulite facies, garnet-cordierite-sillimanite zone and orthopyroxene zone in the south-west, immediately above the Pichao Shear Zone (Finch et al., 2015). This shear zone thrust this sequence over the Agua del Sapo complex (Fig. 2). The isograds are parallel to the dominant NE-dipping, metamorphic foliation and bedding (Büttner et al., 2005; Finch et al., 2015). The granulite facies rocks underwent extensive partial melting, with peak metamorphic conditions estimated at <6 kbar and 800 ^{o}C (Büttner et al., 2005). Migmatites range from metatexite to diatexite, and are the source of leucogranitic peraluminous plutons and different generations of pegmatites that intrude the area (Büttner et al., 2005; Finch et al., 2015; Toselli et al., 1978; Wolfram et al., 2017). The HT-LP anatectic conditions and magmatism of the Tolombon complex lasted for a notably long period of ~60 Ma, between ~505-500 and ~440 Ma, indicated by zircon and monazite U-Pb geochronology (LA-ICPMS and SHRIMP) of migmatites (Finch et al., 2017; Weinberg et al., 2020; Wolfram et al., 2019).

The dominant foliation is part of a deformation event that thrusted rocks to the west, as indicated by asymmetric kinematic indicators (Finch et al., 2017). It also defines the axial planar foliation of asymmetric isoclinal west-verging folds (F1) with sub-horizontal fold axes trending roughly north-south. Many F1 folds are intruded by leucosomes along the axial plane, indicative of syn-anatectic folding and thrusting (Finch et al., 2017). F1 folds tighten and shearing intensity increases towards the Pichao Shear Zone.

2.2.2 Pichao Shear Zone and Agua del Sapo complex

The Pichao Shear Zone (PSZ) is 3 km-wide and dips moderately NE (Finch et al., 2015). The strain intensity increases towards the footwall reaching ultramylonites that form a band of up to 1 km thick (Finch et al., 2015). The PSZ is characterised by: (i) microstructural features and mineral paragenesis that constrain deformation to between 500-700 ^{o}C variably overprinted by greenscshist facies paragenesis; (ii) pervasive top-to-west kinematics recording thrusting of the hanging wall Tolombon complex over the footwall Agua del Sapo complex; and (iii) porphyroclasts and geochemical signature of mylonites indicative of a diatexite migmatite protolith, similar to those of the Tolombon complex (Finch et al., 2015).

The Agua del Sapo complex in the footwall of this shear zone is comprised not only by Al-rich turbidites like the hanging wall, but also by Ca-rich turbidites that now form Hbl-Ttn-Aln-Ep- bearing rocks (Toselli et al., 1978). Toselli et al. (1978) noticed that unlike the granulite facies of the hanging wall, the immediate footwall of the shear zone comprises amphibolite facies rocks. Piñán-Llamas and Simpson (2009) investigated the structural makeup of these turbidite-derived metamorphic rocks suggesting that they were only deformed during the Cambrian Pampean orogeny. However, Finch et al. (2017) reported monazite U-Pb ages that range between 435-420 Ma, ~20 Myr younger than monazite ages in the hanging wall. This paper focuses on this poorly-investigated complex and its tectonic boundary to the west.

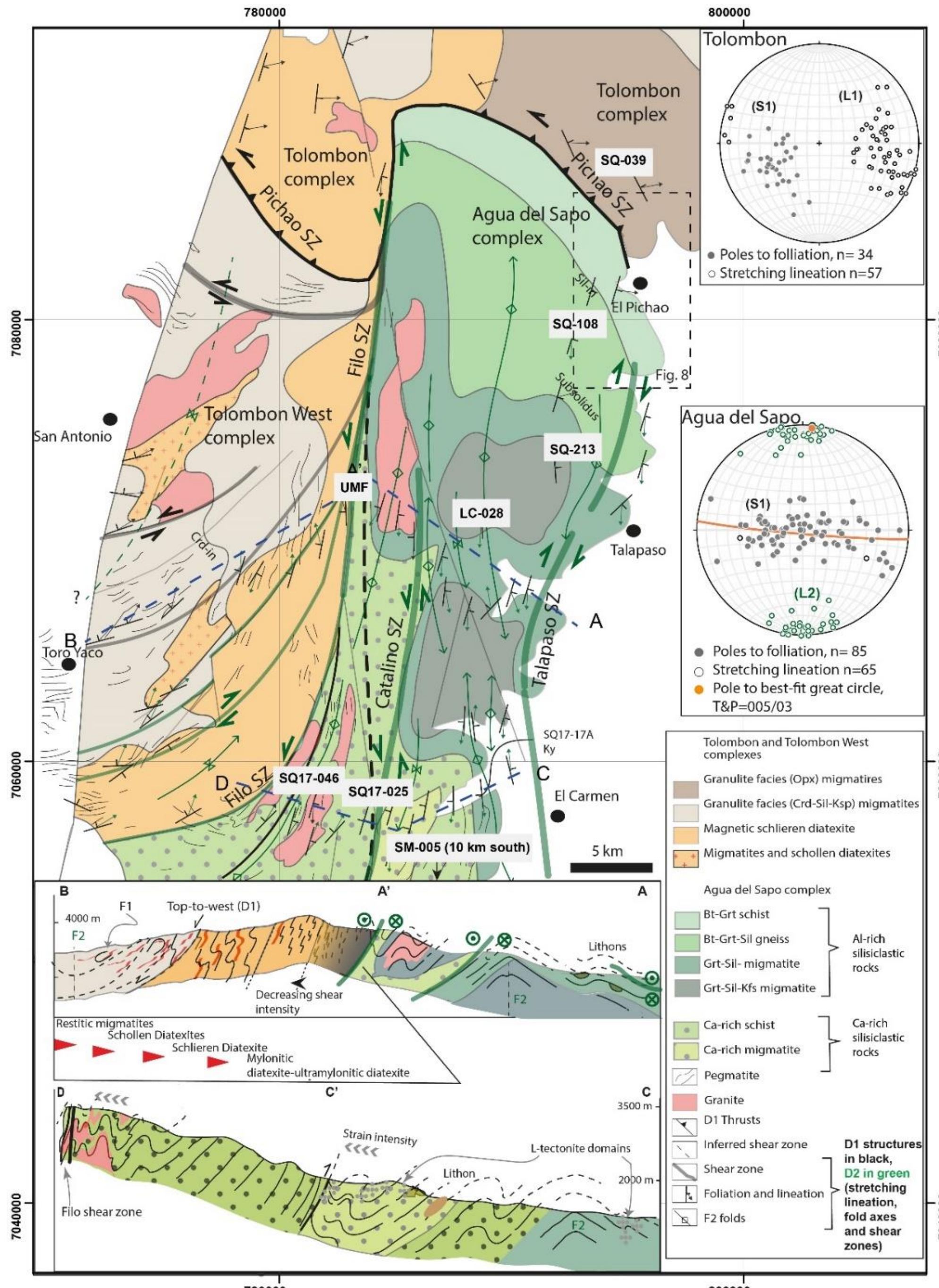

Figure 2. Geological map of the Sierra de Quilmes and its three complexes. Location of titanite samples in labelled grey text box. A-A'-B cross section: dextral and sinistral shear zones and upright folding in the Agua del Sapo complex. C-C'-D cross section: southern section of the Agua del Sapo complex. The strain intensity increases towards the major shear zone in the west recorded by tightening of upright folds.

3 Methods

3.1 Aeromagnetic data

In order to support field mapping efforts, aeromagnetic data were used to interpret structures and major lithological subdivisions. The aeromagnetic survey, designed by SEGEMAR (the Argentinian Geological Service), was commissioned and completed in July 1998. It comprised N-S flight lines with a 1000 m of separation between lines and tie lines every 7500 m. The total magnetic intensity (TMI) grid after corrections was provided by SEGEMAR. The total magnetic intensity grid was processed here to generate the reduced to the pole grid (RTP; Fig. 3a). From the RTP other images were generated using different filters (Fig. 3).

3.2 Crystallographic preferred orientation

In order to determine the nature and temperature of quartz deformation, we analysed the crystallographic preffered orientation (CPO) of quartz-rich rocks. The G50 Fabric Analyser at the School of Earth, Atmosphere and Environment, Monash University was used to measure individual quartz grain c-axis orientation in thin section. The c-axes were used to determine the CPO pattern (Peternell et al., 2010; Wilson et al., 2007). The raw data from the Fabric Analyser was processed in the crystal imaging system *INVESTIGATOR G50 v5.9* software to select the c-axis orientation of specific quartz grains within mono-mineralic quartz ribbons or quartz-rich areas. The quality and accuracy of the data were assessed using two factors for every data point: the geometric and retardation quality. The first is a measure of the closeness of the extinction planes from the different light directions, and the second evaluates the usefulness of the c-axis azimuths. Following procedures in Peternell et al. (2010) and Hunter et al. (2016), values of geometric and retardation quality of <75 were excluded from the analysis. Equal area stereonet diagrams were created for each sample.

3.3 Titanite geochronology

U-Pb dating of titanite was carried out at the School of Earth, Atmosphere and Environment, Monash University, by means of laser ablation ICP-MS in a split stream mode (LASS-ICP-MS). Trace elements, and U-Pb isotopes were analysed for every ablation site. U-Pb isotopes were analysed using a Thermo ICAPTQ triple quadrupole ICP-MS coupled with an ASI Resolution 193 nm excimer laser equipped with a dual volume Laurin Technic S155 ablation cell. Titanite was sampled in a He atmosphere with the laser operating at a repetition rate of 10 Hz and a 25 µm spot size. The laser energy used was approximately 4 Jcm^{-2}. The ablated material fed the ICPMS torches for the U-Pb analysis. Instrumental mass bias, drift, and downhole fractionation were taken into account by analysing standard materials every half hour throughout the analytical session. BLR-1 titanite (Aleinikoff et al., 2007) was used as the primary standard for date calculations, and OLT-1 titanite (Kennedy et al., 2010) as a secondary standard. For trace elements the NIST610 glass was used as primay external standard and the stoichiometric Si content in titanite for internal standardisation. The NIST612 glass, USGS BHVO 2G and BCR 2G were analysed throughout the analytical session to check precision and accuracy of the results.

3.3.1 Zr-in-titanite thermometry

In order to assess (re)crystallisation temperatures in titanite, we used the Zr -in-titanite method using the calibration in Hayden (2008). Analytical uncertainties on Zr measurements are from 5-10 % (2σ) which gives temperature uncertainties of 5-10 ^{o}C. Pressure and activity uncertainties result in even larger temperature uncertainties. Our samples lack rutile and have abundant ilmenite which has an estimated $aTiO_2 > 0.8$ (Chambers and Kohn, 2012; Kapp et al., 2009; Kohn, 2017; Schwartz et al., 2008). Pressure estimates for rocks of the Agua del Sapo complex are not available. Pressure estimates for the surrounding migmatitic complexes (Tolombon and Tolombon West complexes) are in the range of 6-5 kbar (Büttner et al., 2005; Finch et al., 2017). We assume a value of 5.5 kbar for the titanite-bearing migmatites, as suggested by the mineral paragenesis of neighbouring Al-rich migmatites that include cordierite and sillimanite. In an attempt to reflect the uncertainties, we assume a minimum 2σ uncertainty of 25 ^{o}C for each datum.

3.4 Terminology

We follow Sawyer (2008) and use the term *migmatite* for any partially melted rock, *metatexite* for migmatites that preserve the original fabric, *stromatic metatexite* for layered migmatites, *diatexite* for migmatites that lost coherence due to high fraction of melt, *neosome* for rocks that underwent partial melting, *leucosome* for the light-coloured, product of partial melting, and *melanosome* for the residual part of the neosome from which melt was extracted. Mineral abbreviations are after Whitney et al. (2010). When referring to results from geochronology, we use "date" to refer to the calculated value from measured isotopic ratios, and "age" when the date has geological significance (following Horstwood et al., 2016; Schoene et al., 2013).

4 Results

South Sierra de Quilmes: Tolombon West and Agua del Sapo complexes

The region to the south of the Pichao Shear Zone has been split here into two distinct complexes: the Agua del Sapo complex proper, to the east of the mountain divide, and the Tolombon West complex to the west. The two are separated by a newly mapped N-S trending shear zone up to 500m-wide, the Filo Shear Zone, that crops out along the ridge of the mountain and displaces the Pichao Shear Zone sinistrally with a heave of 7 km (Fig. 2). Thus, the three metamorphic complexes in the Sierra de Quilmes - the Tolombon, Tolombon West and Agua del Sapo complexes - are separated by the interconnected Pichao and Filo Shear Zones. This division is based on a combination of geological features and supported by satellite and aeromagnetic images. We start this section by describing the expression of these complexes and bounding shear zones in the aeromagnetic images. We then described these two complexes, their boundaries, lithologies and structures.

4.1 Aeromagnetic images

The aeromagnetic images define two fields with different signatures (Fig. 3), corresponding to the Agua del Sapo complex in the east and the Tolombon West complex in the west. The Agua del Sapo complex is characterised by lower magnetic values and a smoother magnetic texture, with longer wavelength variations in the RTP-TDR and RTP-1VD images, indicating the relatively low dip angles of the stratigraphy. The Tolombon West complex is characterised by a mottled texture in RTP-1VD and RTP-AS images, and stippled in RTP-TDR images. Compared to the Agua del Sapo complex, it has overall higher magnetic intensities (RTP-AS image) and steeper gradients with shorter wavelength patterns, indicating a heterogeneous distribution of magnetic rocks and steeper dip angles.

The difference in magnetic intensity between the two complexes is particularly clear in the south, marking the NE-SW boundary between them. The Pichao Shear Zone in the north is characterised by a low magnetic intensity corridor that contrasts with the higher magnetic values of the granulite facies rocks of the Tolombon complex further to the north.

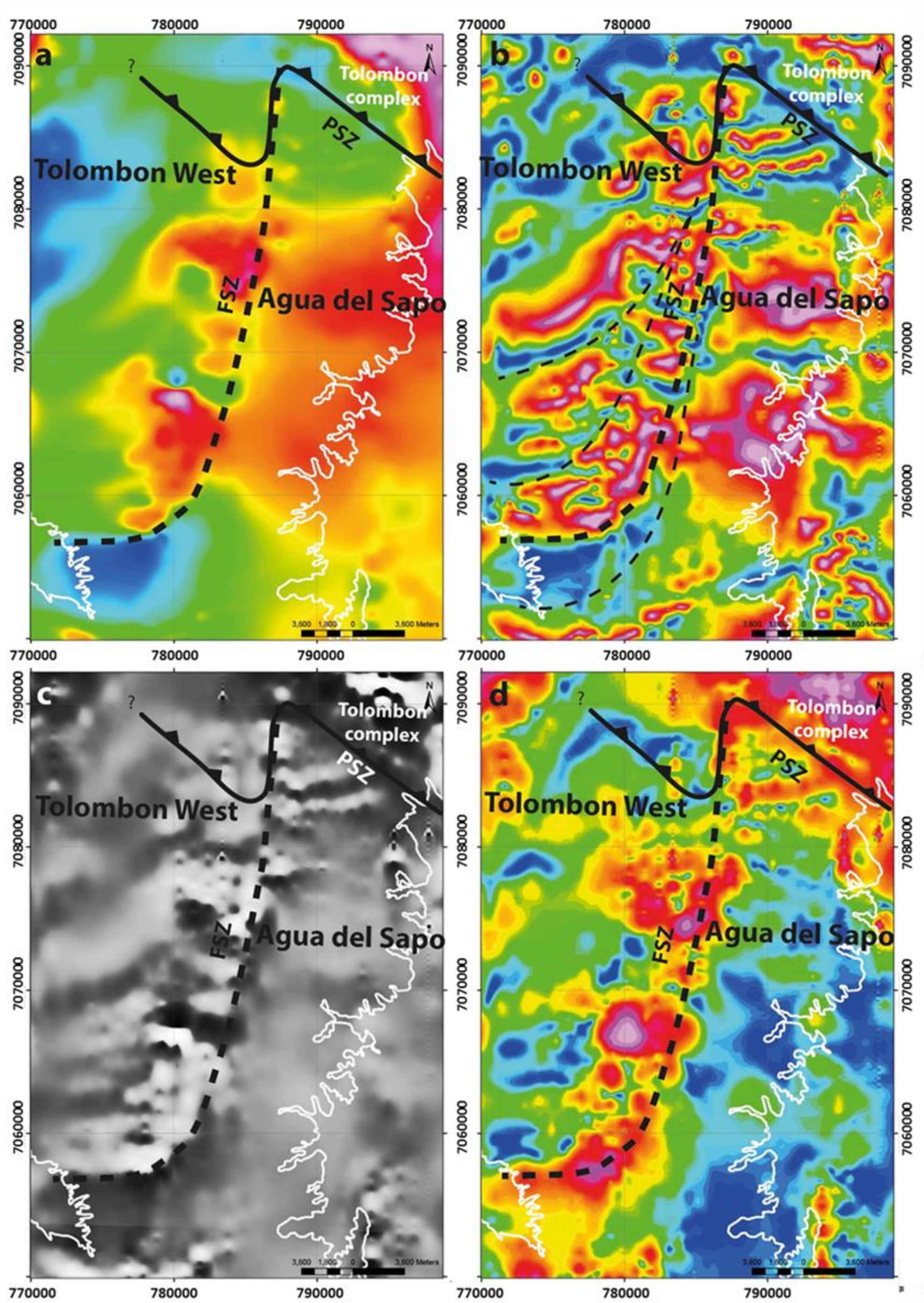

Figure 3. Aeromagnetic images of a section of the Sierra de Quilmes showing the contacts between the three complexes in Fig. 2. a) Total magnetic intensity (TMI). b) Reduced to pole-tilt derivative (RTP-TD). c) Reduced to pole- first vertical derivative (RTP-1VD). Note

the asymmetric magnetic gradient of rocks dipping NW in the Tolombon West complex. d) Reduced to pole- analytical signal (RTP-AS). Note the distinct change in the magnetic signal across the mountain range from west to east, with the Agua del Sapo complex having lower magnetic values in contact with an irregular N-S band of high magnetic rocks following the Filo Shear Zone in the RTP-1VD. Aeromagnetic data provided by SEGEMAR, the Argentinian Geological Service.

4.2 Tolombon West complex

This complex is separated from the Tolombon complex by the western section of the Pichao Shear Zone, and from the Agua del Sapo complex by the Filo Shear Zone (Fig. 2). The rock types here are Al-rich siliciclastic turbidite package with minor calc-silicate rocks, similar to the Tolombon complex, now dominated by migmatites. There is a gradual increase in leucosome volume from west to east, that eventually form irregular granite bodies. This is followed by an increase in finite strain marked by more intense foliation, defined by metamorphic minerals associated with migmatization and reinforced by leucosomes.

In the west, migmatites are melanocratic, restitic metatexites interlayered with 5-10 m wide bands of nebulitic metatexites and mesocratic schollen diatexites. The restitic metatexites are folded and preserve the original compositional layering of the turbiditic protolith. Where restitic metatexites dominate, there are regularly-spaced lenses of leucosome subparallel to the axial surface of N-S trending folds (Fig. 4a). These restitic metatexites are dominated by biotite, cordierite, sillimanite, plagioclase, and K-feldspar with ~20 modal % of quartz and rare scattered garnet (Fig. 4b).

Towards the east, the metatexite transitions to diatexite. This is coupled with the disappearance of cordierite and an increase in modal content of garnet. There are, however, round nodules of Sil+Bt+Grt that could represent pseudomorphs after cordierite (Fig. 4b). In this area, as in the Agua del Sapo complex, there are leucosomes of tonalitic composition crosscutting migmatitic bedding (Figs. 4d and 4e). Unlike other rock sequences, here magnetite-rich diatexite migmatites dominate (Fig. 2). They are associated with pegmatites with 5 cm-wide patches of magnetite, and are reflected in the high magnetic susceptibility values of this area (Fig. 3). Pegmatites and irregular granitic bodies are broadly parallel to the main foliation (Fig. 2). The large San Antonio granite stock in the north of the complex is a leucogranite hosted by Crd-bearing schists and characterized by magmatic layering defined by tourmaline, biotite and garnet.

The migmatites across the Tolombon West complex have a garnet-cordierite-sillimanite paragenesis, similar to parts of the neighbouring Tolombon complex, suggesting temperatures between 650-750 ^{o}C and pressures below 5 kbar (Büttner et al., 2005). Unlike the Tolombon complex, there is no evidence of granulite-facies conditions marked by the presence of orthopyroxene. Rocks of the Tolombon West complex are marked by a strong retrogression of peak metamorphic assemblages where cordierite and garnet are partially replaced by biotite-sillimanite (Fig. 4b), and sillimanite and K-feldspar are commonly replaced by 2-3 cm poikiloblasts of muscovite, commonly randomly oriented.

4.3 Agua del Sapo complex

The Agua del Sapo complex in the footwall of the Pichao Shear Zone and east of the vertical Filo Shear Zone (Fig. 2) encompasses a suite of strongly deformed metasedimentary rocks. The bulk composition and the metamorphic grade of these rocks vary from north to south. In the north, in the immediate footwall of the PSZ, the rocks are garnet-biotite schists and sillimanite paragneisses of amphibolite facies similar to the sub-solidus rocks of the Tolombon complex. The transition from schist to paragneiss is coupled with the first appearance of sillimanite (Fig. 4e), which increases in modal content towards the south. Approximately 10 km south of the PSZ, near Talapaso village (Fig. 2), metatexite migmatites mark the onset of partial melting evidenced by discrete 2-5 cm-wide leucosome lenses at high angle to bedding (Fig. 4f). The change in metamorphic grade is marked by a southward increase in magnetic values visible in Figs. 3a, b.

Some 20 km south of the PSZ, these rocks grade to Hbl+Ep+Aln+Ttn-bearing metasedimentary rocks (Fig. 4h). We refer to these rocks as Ca-rich siliciclastic rocks. They have interlayered pelitic and psammitic beds preserving graded bedding, and are interpreted to represent metamorphosed turbidites. The onset of partial melting in these rocks (marked in Fig. 2) is indicated by discrete leucosomes and increase in grain size to an average of 1-2 mm, with only minor changes in the bulk mineralogy, as well as the appearance of clinopyroxene and rare Ca-rich scapolite (meionite). They typically have variable but limited volumes of leucosome (up to 10-15% in area) (Fig. 4g).

Peraluminous two-mica granites, are common in the vicinity of the FSZ (Fig. 2). These granites are elongated north-south, weakly foliated and concordant with the country-rock foliation. The mineralogy includes garnet, biotite, sillimanite and muscovite, with accessory zircon, monazite, and rare apatite.

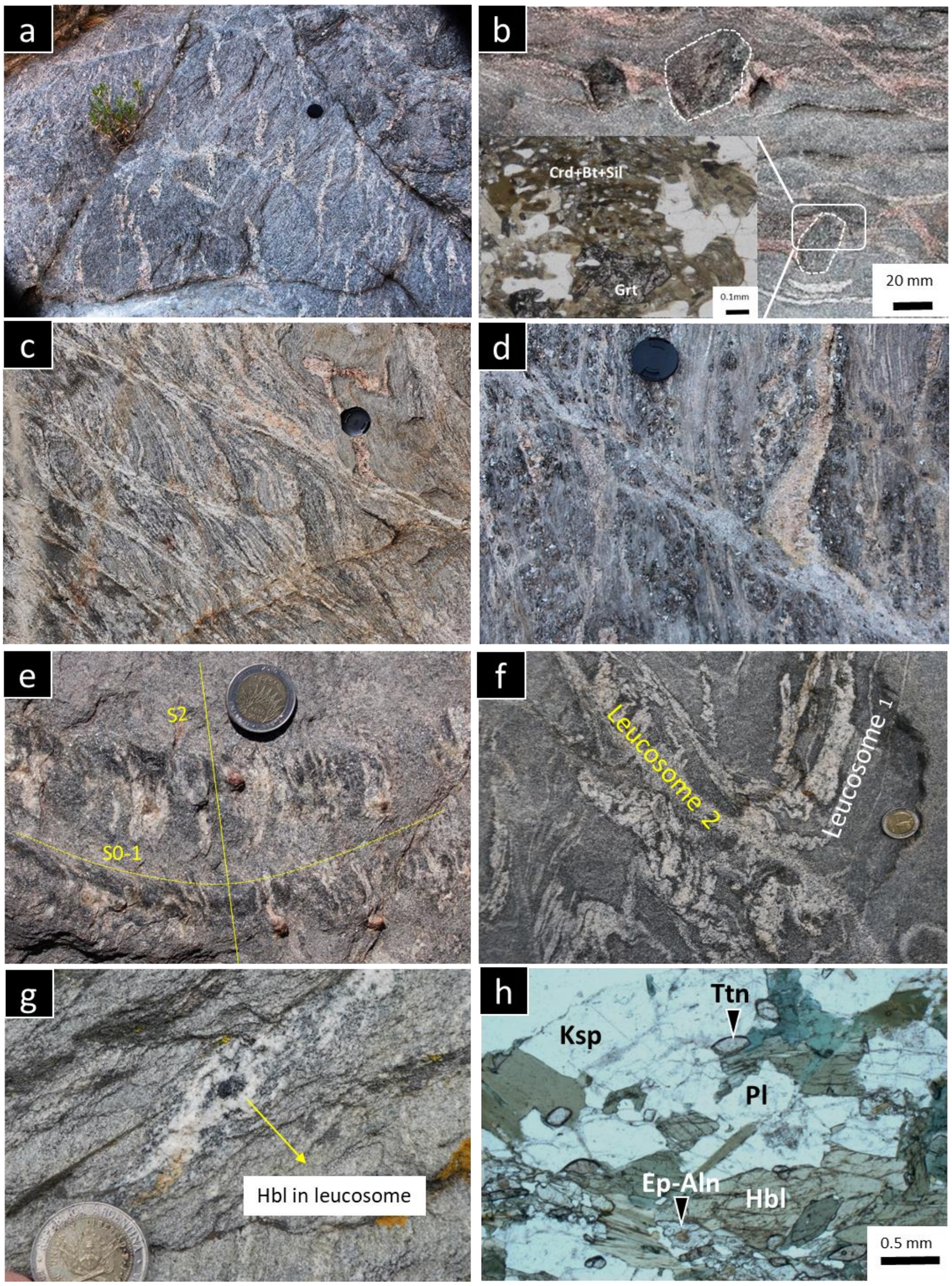

Figure 4. (a-d) Tolombon West migmatites. (a) Restitic migmatite with a set of regularly spaced leucosomes 20-25 cm long, oriented sub-parallel to the axial surface of folds (vertical in the photograph) and at an angle to the dominant foliation. (b) Retrogressed cordierite porphyroblasts up to 5 cm across, now biotite-sillimanite-cordierite cored by garnet (inset photomicrograph). Note the thin leucosome surrounding and connecting porphyroblasts forming a layer. (c) Thin leucosomes in shear planes parallel to the Filo shear zone. (d) Two sets of leucosome overprint each other in migmatite: early, foliation-

parallel granitic leucosomes are overprinted by later, thinner tonalitic, net-veined leucosomes. (e-f) Agua del Sapo Al-rich siliciclastic rocks. (e) Grt-Bt-Sil aggregates aligned parallel to S2, at a high angle to bedding. (f) Two sets of leucosome overprint each other in migmatite: leucosome 1 is parallel to bedding with a melanosome rim, and leucosome 2 crosscuts all structures and has diffuse margins against host rocks. (g-h) Agua del Sapo Ca-rich siliciclastic rocks. (g) Qtz+Mc+Hbl leucosome in sheared migmatite where the neosome comprises Hbl+Pl+Ep+Aln+Ttn+Ksp. Peritectic Hbl is larger and euhedral when compared to Hbl grains in neosome. (h) Typical mineral paragenesis and texture of Ca-rich migmatite.

4.4 Structures

The ductile structures of the Tolombon West and Agua del Sapo complexes provide a complementary record to that of the Tolombon complex where west-verging thrusts and folds were coeval with anatexis (Finch et al., 2017). The structural record of the Tolombon West is markedly different from that of the Agua del Sapo, being dominated by folds with local shear zones, whereas the Agua del Sapo complex is dominated by a very distinctive prolate deformation with an intense stretching lineation and intense simple shear deformation.

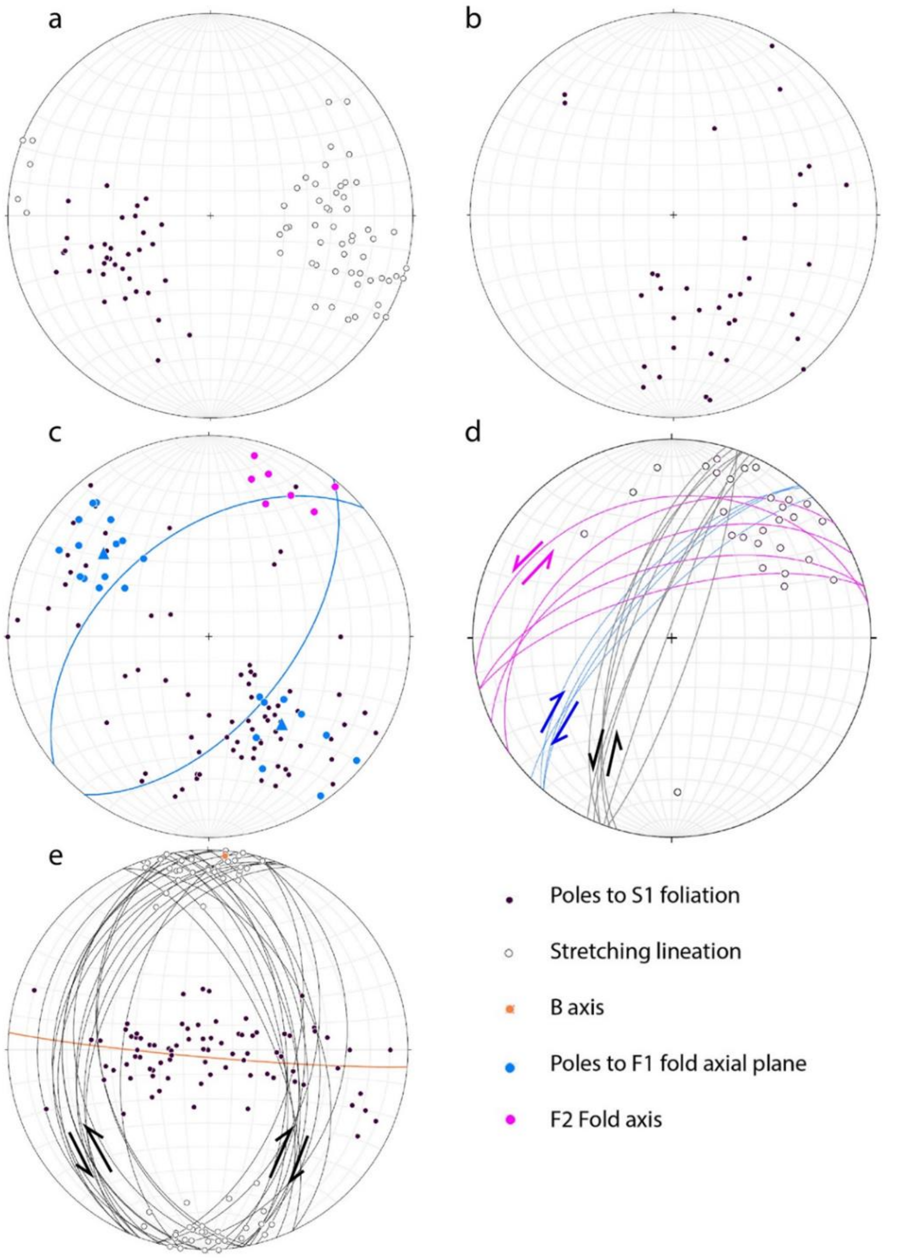

Figure 5. Stereonet projections of foliation and lineation from the Sierra de Quilmes. Data from: (a) Tolombon complex showing a well-defined lineation associated with W-verging thrusts (data from {Finch, 2015 #259}). (b) North section of the Tolombon West. The west-dipping foliation is from areas near the Filo shear zone and the north-dipping foliation from the west side of the complex. (c) South part of the Tolombon West complex. Poles to fold axial planes with leucosomes (blue dots) are parallel to S1 (black poles), and cluster in two groups indicating two limbs of F2 folds. Blue great circles are the mean plane from each pole cluster which intersect in the NE, close to shallow plunging F2 fold axes. (d) Shear zones in Tolombon West complex. Blue great circles indicate dextral shear zones, purple indicates sinistral shear zones and black indicates the sinistral splays from the Filo shear zone. (e) Agua del Sapo complex. Black great circles represent shear zones: dextral when dipping to the east and sinistral when dipping to the west. Together they define limbs of F2 folds and their B axis is parallel to the stretching lineation.

4.4.1 Structures in the Tolombon West complex

The Tolombon West complex, bound by the two shear zones (Fig. 2), can be divided into a northern and the southern section based on structural style. The limit between the two is diffuse and around the town of Toro Yaco (Fig. 2). The structures in the northern section are similar to those of the Tolombon complex (Fig. 5a), dominated by syn-anatectic fold and thrusting to the west. The dominant foliation, S1, is parallel to bedding (Fig. 5b), associated with F1 isoclinal folds and top-to-west shear zones. Foliation strikes N-S and dips west near the FSZ, and rotate to a NE-SW trend, dipping NW, away from the shear zone. F1 folds are associated with leucosomes parallel to the axial planes (Fig. 6a), suggesting that the folds were syn-anatectic. Unlike the Tolombon complex, there are sinistral shear zones dipping moderately to the NW with a mineral lineation, mostly sillimanite, that plunges between 10-30^{o} NE. These are relatively narrow (2-5 m wide) mylonitic to proto-mylonitic shear zones, and a few of them have 20-30 cm thick ultramylonitic bands. The presence of sillimanite on the shear planes indicates high-grade metamorphic conditions, as with the thrusts in the Tolombon complex (Büttner et al., 2005; Finch et al., 2015). In the west, where S1 dips NW, there are metric-scale N-S trending, upright, open folds with leucosomes in their axial planes, parallel to a new S2 foliation, related to a second folding event (F2).

In the southern section, the fabric rotates from N-S to NE-SW following the curved trace of the Filo Shear Zone (Fig. 2). The F1 isoclinal folds rotate with the foliation, and like the northern section, they typically have axial planar leucosome veins and cuspate fold hinges (Fig. 6a), and are sub-parallel to S1. However, unlike the northern section, F1 and S1, are overprinted by km-scale upright F2 folds plunging 5-10^{o} to the NE, and an inter-limb angle of ~75^{o} (Fig. 5c). The axial planar foliation, S2, is defined by elongated porphyroblasts of the high-temperature minerals cordierite, fibrolite sillimanite, and biotite. In some places, S2 is coupled with leucosomes showing continued anatexis (Fig. 6b).

In the south, there are also shear zones parallel to S1, however their kinematic is variable. Some 5 km to the south of Toro Yaco town (Fig. 2) there are 1-2 m-thick sillimanite-bearing dextral shear zones that dip ~70^{o} NW and overprint F2, deflecting their trace by a few centimetres. To the east and south of these dextral shear zones, there are sub-vertical sinistral shear zones that are part of the splays of the Filo Shear Zone. Both sets of shear zones are parallel to the F2 axial planes and their mineral stretching lineation, mostly defined by sillimanite and stretched mineral aggregates, plunge ~30° NE (Figs. 2 and 5d).

4.4.2 Filo Shear Zone

The trace of the sub-vertical Filo Shear Zone in the aeromagnetic images (Fig. 3) defines a broad, curved shape, similar to the S1 foliation described above, rotating gradually from a north-south to an east-west orientation, where it ends as numerous splays in the south marked by the 2-5 m-thick mylonitic bands described above (Fig. 2). In the northern section, its width is ~500 m and records intense deformation producing a ~200 m thick black, ultramylonitic rock with naked clasts, similar to those in the Pichao Shear Zone (Fig. 6c). Further to the north it displaces and merges with the Pichao Shear Zone (PSZ) deflecting it by~ 7 km sinistrally. Its sinistral kinematics is indicated by σ-shaped prophyroclasts of feldspar and garnet, muscovite fish, and shear bands formed by biotite-sillimanite (Fig. 6c). Along most of its length, the mylonitic rocks have lower amphibolite facies paragenesis, and deforms both the Al-rich and the Ca-rich siliciclastic rocks of the Agua del Sapo complex, including rocks with stretched hornblende, epidote and allanite. Where it merges with the Pichao Shear Zone, there is a greenschist facies overprint with chlorite in the matrix (see also Finch et al., 2015). In this region, the core of the shear zone has a gently NNE-plunging lineation in a subvertical sinistral shear zone. Outwards from this core zone, the lineation rotates towards W- or E-plunging, and the ultramylonitic foliation becomes moderately dipping recording top-to-W motion, suggesting that the earlier, top-to-West Pichao Shear Zone was rotated and overprinted by the sinistral motion of the Filo Shear Zone.

The ultramylonite of the FSZ is typically characterised by a matrix that is reasonably homogeneous with only short quartz ribbons (Kilian et al., 2011) while the Kfs porphyroclasts are mantled by recrystallized K-feldspar and myrmekites. Quartz shows dominant recrystallisation by grain boundary migration (GBM) and strong crystallographic preferred orientation (CPO) (Fig. 6e and f). Quartz also shows evidence for bulging (BLG) (Fig. 6d).

4.4.3 Structures in the Agua del Sapo complex

Deformation in the Agua del Sapo complex is different from the other complexes. The Agua del Sapo complex is dominated by intense shearing with top-to-south transport (Fig. 7a,b and d) and an intense N-S trending lineation (Fig. 7e,f). These structures overprint earlier ones preserved in lithons, that are typical of the hanging wall Tolombon complex (D1), and therefore mark a D2 event. This is the last major event and is followed by a much weaker D3 event represented by a set of 1-5 m wide, sub-vertical greenschist facies dextral shear zones striking north-south, in the eastern edge of the complex (Fig. 2). Here, we describe the two major deformational events in this complex.

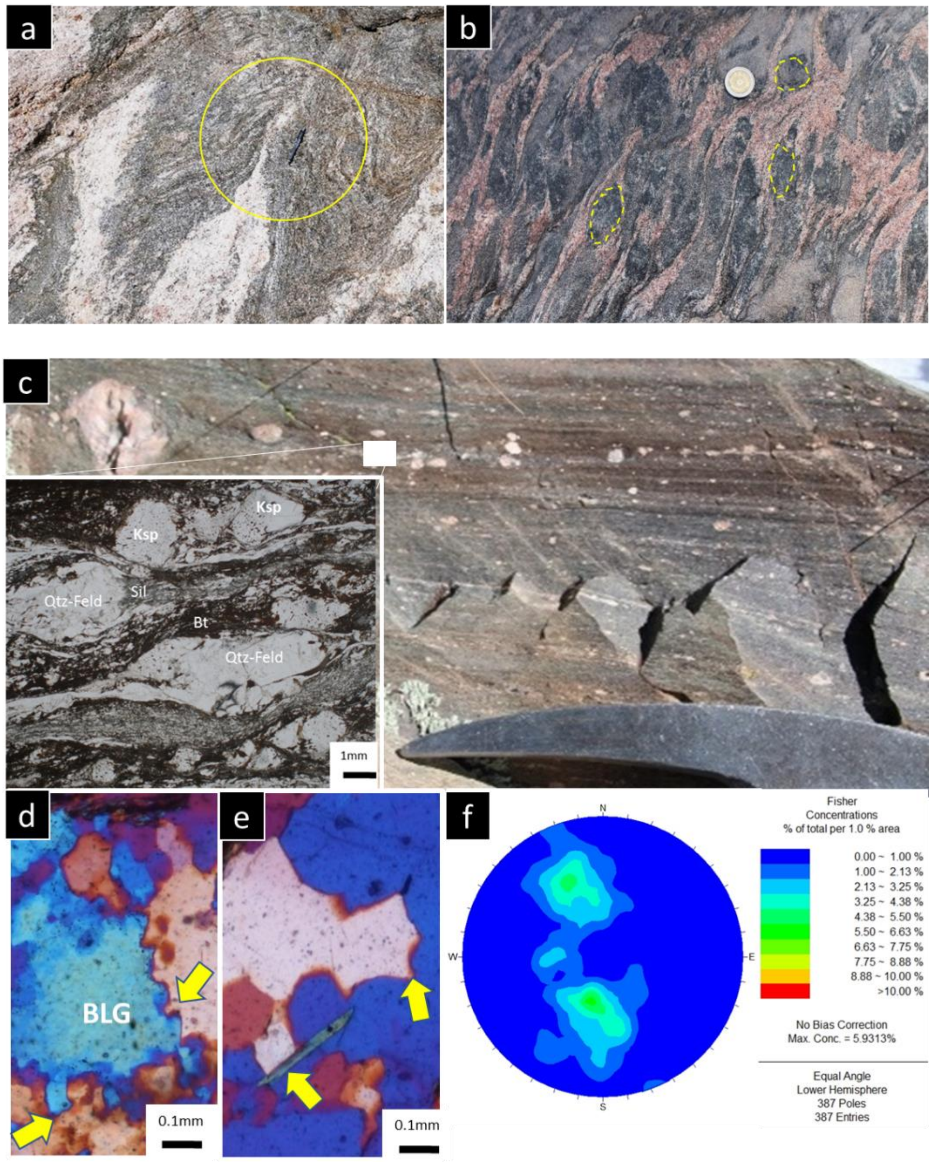

Figure 6. (a-b) Structures in the Tolombon West complex. (a) F1 cuspate hinge in isoclinal folds with leucosome on the axial surfaces. (b) Leucosome controlled by S2, wrapping

around large cordierite porphyroblasts, marked by yellow dashed ellipses. (c-f) Filo Shear Zone. (c) Ultramylonite hand-sample with photomicrograph in plane-polarized light (inset). Quartz-feldspar aggregate form clasts with recrystallized tails parallel to bands of biotite-sillimanite. (d-f) Photomicrographs with cross-polarized light and gypsum plate representing samples of shear zones. (d) Lobate margins of recrystallised quartz, suggesting the onset of bulging (BLG). (e) Grain boundary migration (GBM) of quartz evidenced by cuspate and lobate borders and pinning by mica grain (yellow arrows). (f) Stereogram of quartz c-axis orientation from the FSZ mylonite showing strong preferred orientation defining two maxima that define a weak girdle.*

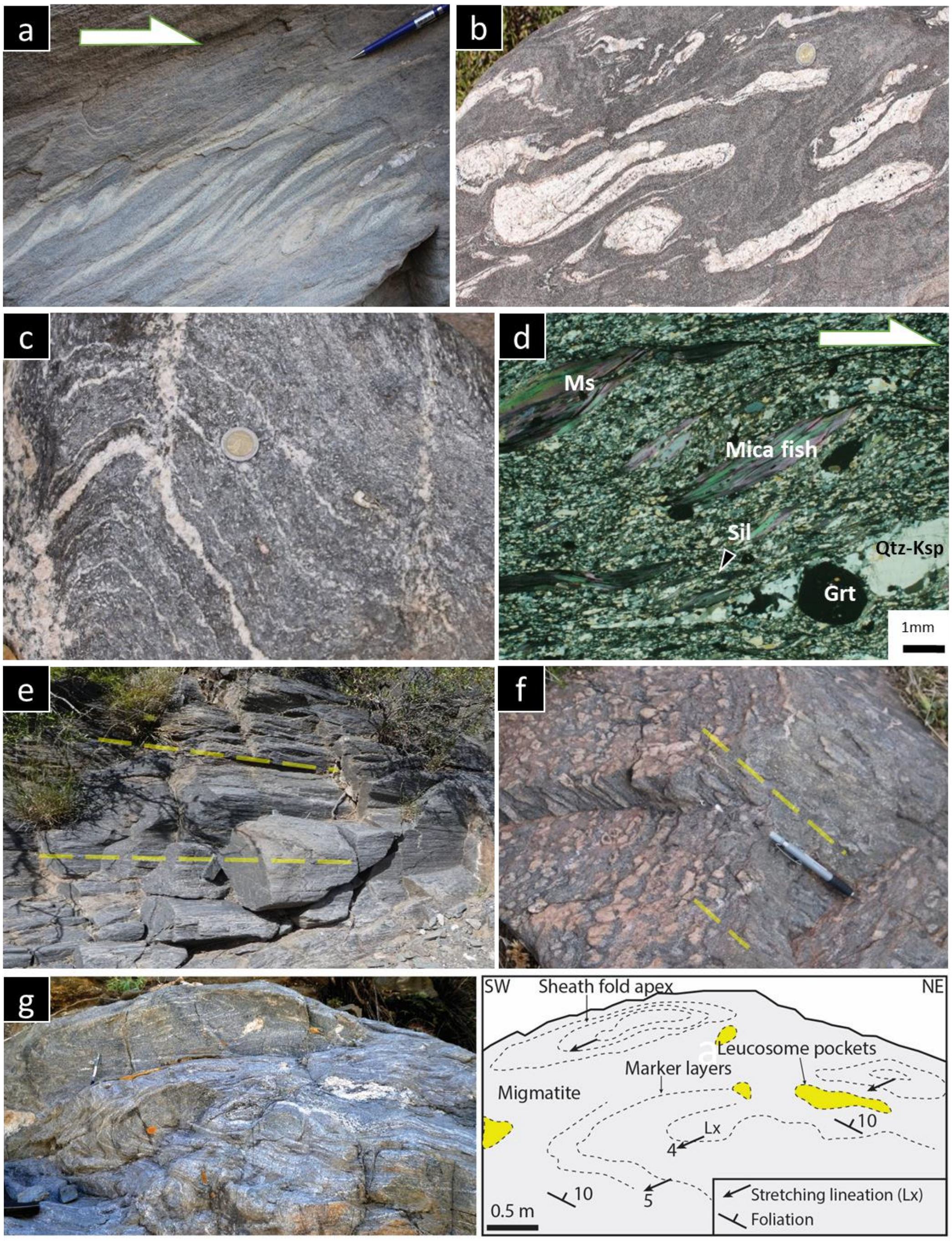

*Figure 7. Structures of the Agua del Sapo complex. (a) Tight fold train with vergence to the right (top-to-south) in amphibolite facies metasedimentary rock. (b) Same for strained and partly disaggregated pegmatites in psammite. (c) Upright F2 fold with leucosome in axial

planar foliation. (d) Photomicrograph of a schist showing dextral motion (top-to-south) indicated by mica fish and asymmetric tails around garnet. (a, b and d) are parallel to lineation and perpendicular to foliation and consistently indicate top-to-south. (e-f) L-tectonites in different rock-types: e) Metapsammite. f) Metapelite with stretched quartz and feldspars showing the absence of a foliation. (g) Sheath folds parallel to stretching lineation and diagram to the right showing details. Leucosomes are either folded with the dominant foliation or form pockets elongated parallel to fold axis and Lx.

D1 structures

The earliest structure in this complex is a metamorphic foliation parallel to bedding (S1), that is only preserved in lithons. These lithons occur in the north (Fig. 8) and their size and frequency decrease to the south, where D2 becomes more intense. S1 is defined by muscovite, biotite and sillimanite in the Al-rich siliciclastic rocks, and biotite and hornblende plus elongated epidote-allanite grains in the Ca-rich ones. Leucosomes are axial planar, and cross cut the hinge of isoclinal folds (F1) suggesting that folding was contemporaneous to peak metamorphism and anatexis. Stretching lineation plunges east and is associated with top-to-west kinematics. Thus, D1 structures are similar in orientation, high-grade paragenesis and kinematics to structures in the Tolombon complex. The transition between lithons and rocks dominated by D2 structures is sharp, and defined by the progressive rotation of the stretching lineation over 1 to 2 metres across strike.

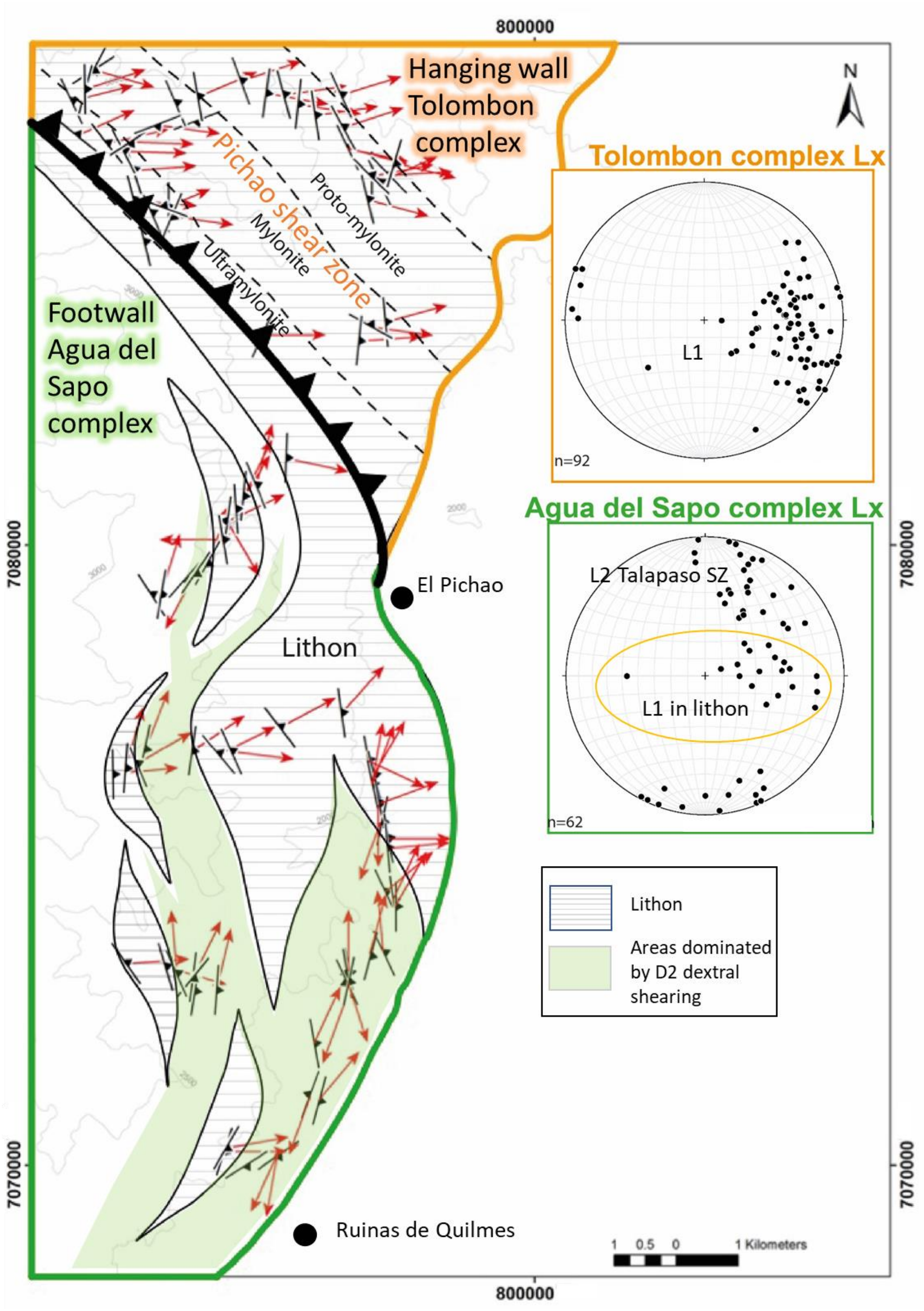

Figure 8. Lithons in the footwall Agua del Sapo complex below the Pichao Shear Zone. Green fields are regions dominated by strongly deformed rocks (D2) marked by dextral shearing along sub horizontal lineations defining the Talapaso SZ (Fig. 2) and horizontal stripes mark less deformed lithons preserving the older top-to-west sense of shear dominant in the Tolombon Complex and the Pichao Shear Zone with E-plunging lineations. Stereographic projections show stretching lineation measured in the Tolombon and Agua del Sapo complex.

D2 structures

Shear zones and stretching lineation (L2)

The Agua del Sapo complex is generally strongly sheared with a well-defined lineation sub-horizontal N-S that can be seen from a distance (Fig. 2). Given the rock types, particularly the psammites, it is not always possible to ascertain strain intensity. However, markers like pegmatites and leucosome veins are strongly stretched or folded (Fig. 7a-b) and tend to be mylonitic, indicative of high-strain zones. We have tentatively defined two main high-strain corridors parallel to the Filo Shear Zone: the Talapaso Shear Zone to the east and the Catalino Shear Zone to the west (Fig. 2 and 8). They both have the same dominant horizontal, N or S plunging stretching lineation. The Talapaso Shear Zone dips ~45^{o} E and has a dextral shear sense, whereas the Catalino Shear Zone dips ~35-40^{o} W and has a sinistral shear sense. Thus, they both record top-to-the-south kinematics. Like the Filo Shear Zone, the Catalino Shear Zone seems to merge with the Pichao Shear Zone. The Talapaso and Catalino Shear Zones are typically 500 m wide mylonitic zones that transition into proto-mylonites across strike. The strain profile in these shear zones is asymmetric with a sharp strain gradient in the footwall and a wider gradient towards the hanging wall. In between these major shear zones, there are several parallel proto-mylonitic corridors with consistent top-to-south movement, independent of their dip direction. The most typical kinematic indicators are asymmetric shear folds (Fig. 7a-b), σ-shaped porphyroclasts of feldspars, muscovite fish (Fig. 7d), asymmetric strain shadows around garnet and other mineral aggregates, and C' shear bands formed by biotite-sillimanite. The mineral lineation (L2) plunges 0 to 10^{o} to the north or south (Fig. 5e), and is defined by elongated quartz-feldspathic aggregates, micas, and tourmaline.

The strongly strained pegmatites and leucosomes in the shear zones have both quartz and feldspars ductily stretched. Quartz is recrystallised by sub-grain rotation (SGR), characterised by a strong oblique fabric defined by new grains or well-defined undulose extinction (Passchier and Trouw, 2005). There are also quartz ribbons along the main mylonitic foliation and areas where quartz crystals have straight grain boundaries and lack undulose extinction indicative of static recrystallisation, or grain boundary area reduction (GBAR similar to that in Fig. 6e). Feldspar porphyroclasts are mantled by fine recrystallised grains and have myrmekites where it faces the shortening direction.

Upright folds (F2)

The opposite dip directions of the two major shear zones described above, as well as changes in the broader foliation distribution define km-scale N-S trending upright folds (F2) (Fig. 5e). These are also present at smaller scale (Fig. 7c), similar to the ones in the southern Tolombon West complex. In the east of the Agua del Sapo complex, they are open folds, with a 2-5 km wavelength, grading to close folds with a 0.5-0.1 km wavelength in the west, near the Filo Shear Zone. The intensity of S2 axial planar foliation also increases westwards, coupled with the tightening of fold inter-limb angle (lower cross section in Fig. 2). The F2 fold axis is parallel to the stretching lineations (L2) in the shear zones and plunges gently north or south, defining large-scale doubly-plunging folds or elongated domes (Fig. 2). The core of these domes expose the highest grade rocks in the complex, and coincide with the two large magnetic anomalies in the RTP_TD (Fig. 4). The axial planar foliation (S2) cross-cuts S0/S1 (Fig. 4e) and can be observed at scales from satellite to microscopic. S2 is defined by biotite and sillimanite, and L2 by elongated mineral aggregates (Bt-Sil rimming Grt) parallel to the fold axes. In relatively rare outcrops, the F2 axial plane has leucosome veins (Fig. 7c) suggesting that incipient anatexis occurred during D2.

L and L>S tectonites and sheath folds

In between the Talapaso and Catalino Shear Zones, there are kilometric domains characterized by L- and L>S tectonites (Fig. 7e-f) dominated by a N-S, low pitch stretching lineation. In these rocks, long minerals such as amphibole, tourmaline and sillimanite, define a lineation whereas the basal cleavage of micas lack preferred orientation. They are commonly associated with sheath folds (Fig. 7g), variable in size (0.5 to 3 m) and shape, and stretched parallel to L-tectonites, many with acute hinge angles, lower than 20^{o}. This tight sheath folds are classified as tubular folds (Skjernaa, 1989) and here they have their fold hinge pointing to the south.

Quartz crystallographic preferred orientation (CPO)

In order to determine whether the linear fabric is a result of constriction or another mechanism, such as overprinting deformation phases (Ramsay and Huber, 1983), we analyzed the crystallographic preferred orientation (CPO) of quartz-rich bands (> 90% quartz) of L-tectonites (Heilbronner and Tullis, 2006; Pennacchioni et al., 2010). The CPO pattern for quartz-rich layers shows cleft-girdles or a vertical single-girdle (Fig. 9a and b, respectively). The difference between those two patterns reflects the variable c-axis opening angle, which increases as a function of deformation temperature, as rhomb <a> and basal <a> slip become more important (Sullivan and Beane, 2010). Figure 9a shows a quartz c-axis CPO pattern that correspond to constriction, and Figs. 9b and c show similar contrictional pattern with a slightly oblique single-girdle, typical of simple shear(Lister and Hobbs, 1980; Sullivan, 2009, 2013). The oblique single-girdle suggests that quartz was affected by a component of non-coaxial deformation (Lister and Hobbs, 1980; Passchier and Trouw, 2005; Sullivan and Beane, 2010). In samples with >10 % mica, the CPO pattern becomes diffuse most likely because of the influence of other phases in pinning quartz and modifying local conditions (Hunter et al., 2016)(Fig. 9d and 9e).

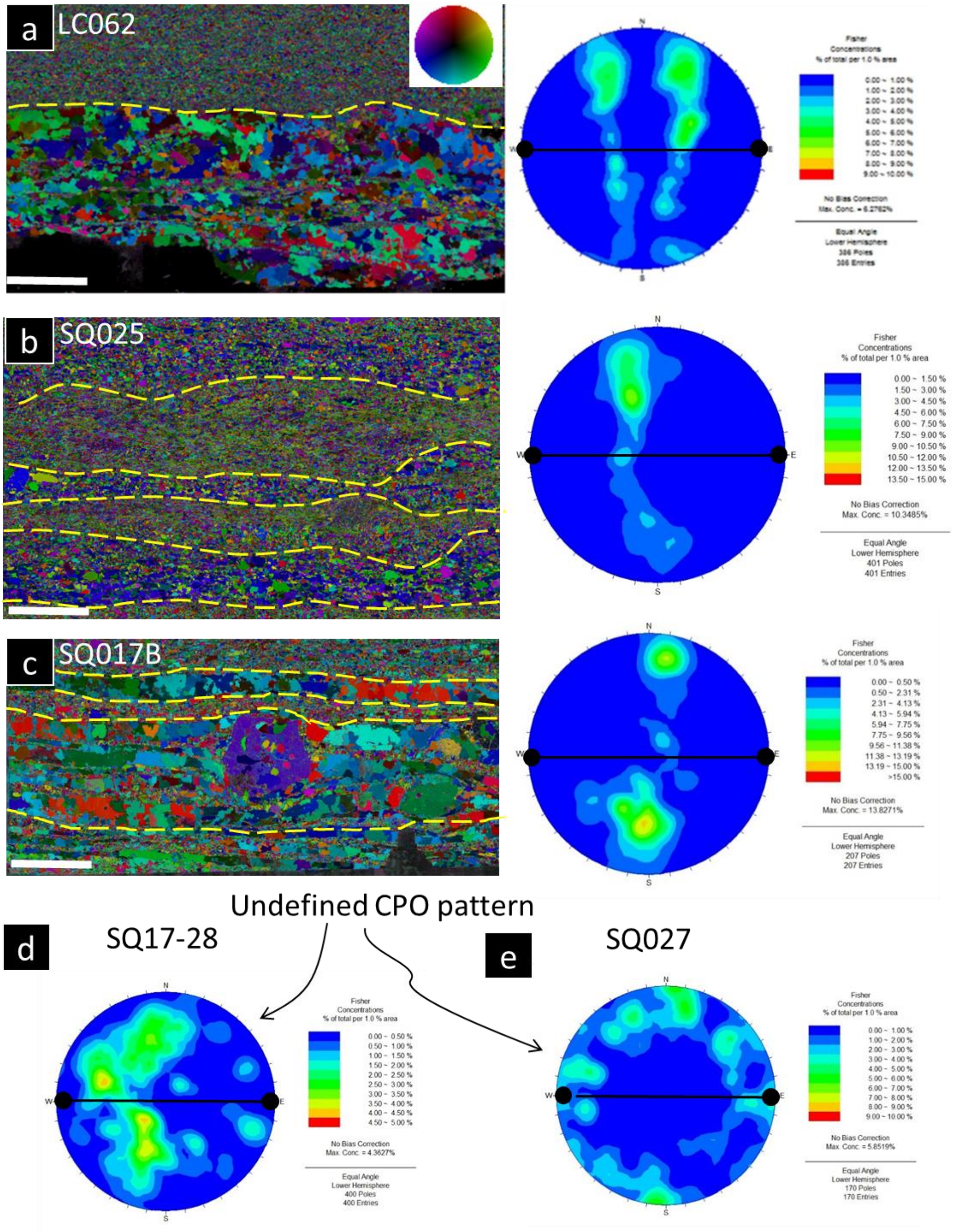

Figure 9. CPO pattern for samples of quartz-rich L-tectonites. Data collected in thin sections cut parallel to lineation and perpendicular to the foliation. (a-c) C-axis orientation image of thin sections to the left and stereograms of the c-axis to the right. The colour of every grain represents its c-axis orientation in space (top right corner colour-coded circle). The sections analysed in every sample are the coarser-grained quartz-rich layers marked by yellow dashed lines. These layers contained < 10 % of other mineral phases and are several quartz grains in width. The reference frame in the stereograms is defined by the E-W vertical foliation plane (black line) and the horizontal lineation represented as black dots. (a) This sample shows two parallel single-girdles or "cleft girdle" typical of constrictional strain. (b, c) Slightly oblique single-girdle, typical of simple shear. (d-e) Stereograms from samples with > 10% mica and feldspar showing ill-defined CPO (d), or no CPO pattern at all (e).

4.5 Titanite geochronology

LASS-ICP-MS spot analysis was conducted for titanites from seven different Ca-rich siliciclastic rocks, some in-situ and some from mounted separates (Supporting information). An eight sample, of calc-silicate sample from the granulite facies rocks in the Tolombon complex (sample SQ-039) was analysed for comparison (Büttner et al., 2005). Most of the titanite grains are 100-150 µm in size, euhedral to subhedral with aspect ratios between 1 and 4. The corrected $^{207}Pb/^{206}Pb$ date of every spot was defined as the lower intercept of the anchored Discordia line with the Concordia in a Tera-Wasserburg diagram. The Discordia is also anchored to a $^{207}Pb/^{206}Pb$ value of 0.86 based on the model evolution of Stacey and Kramers (1975) for ~470-440 Ma. To visualize the dates distribution the corrected $^{207}Pb/^{206}Pb$ dates were plotted in a probability plot (Fig. 10a).

The seven titanite-bearing samples analysed from the Agua del Sapo complex are similar amongst them. They share the same grain-size between 0.2-0.5 mm, and mineralogy (Qtz+Hbl+Bt+Kfs+Pl+Ms+Ep with Cal+Ap+Ttn+Aln+Ilm as accessory phases), which is suggestive of similar peak metamorphic conditions. They all show similar structures, marked by a well-defined foliation defined by aligned hornblende, epidote and micas. All, except SQ-108, were collected in areas with evidence of anatexis (Fig. 2). Finally, they al show minor retrogression, marked by minor chloritization.

Despite the general similarities between the Agua del Sapo samples, the results define three groups, with different titanite U-Pb date populations (Fig. 10a). Samples SQ17-025, UMF, and SQ17-046C define a unimodal age distribution spread between 500 and 440 Ma, with few spots younger than 440 Ma. In contrast, samples SM-005 and SQ17-028 yield a broad peak of younger ages, ranging between 440 and 380 Ma, with fewer spots older than 440 Ma. The remaining two samples, SQ-213 and SQ-108, cover most of the range defined by these two groups (inset in Fig. 10a). Titanite from sample SQ-039, from the Tolombon complex, yields dates in the range 480-440 Ma, reinforcing the dates in Büttner (2005) (Fig. 10a).

Zr-in-titanite temperature

The results for Zr-in-titanite thermometry in Fig. 10b show that estimated temperatures are generally above 700 ^{o}C for the entire range of dates recorded by titanite. Temperature increases with time from 700 ^{o}C at ~500 Ma reaching a broad maximum in excess of 750 ^{o}C at ~460 Ma, and then decreases steadily to ~700 ^{o}C ending at 380 Ma (Fig. 10b). Sample SQ-039 from the Tolombon complex differes from the rest, with higher values and a weighted average temperature of 809.4 ± 3.7 °C, in accordance with the estimated peak metamorphic conditions for the complex (Büttner et al., 2005). Zr-in-titanite data are provided in the supporting information.

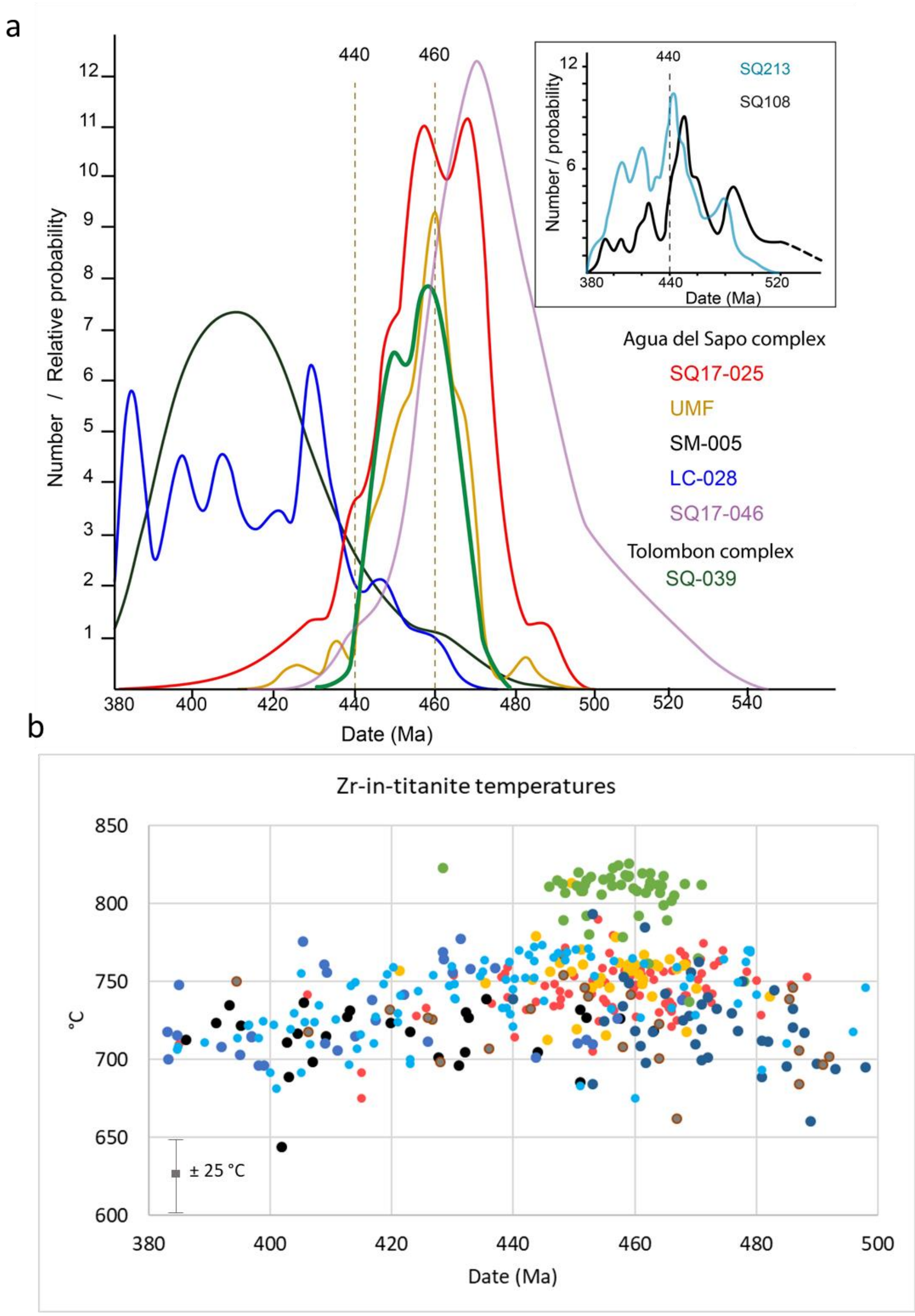

Figure 10. (a) Titanite U-Pb dates summarized in a probability plot. Sample SQ-039 from Tolombon complex yield dates between 480-440 Ma. For the Agua del Sapo complex, titanites from SQ17-025, UMF, and SQ17-046 yield dates in the 540-440 Ma range, while LC-028 and SM-005 have most dates in the 440-380 Ma range. Samples SQ108 and SQ213, in inset, have a much larger spread of dates (> 120 Ma), overlapping with all other samples in the complex. (b) Zr-in-titanite temperatures from the same analytical spots in (a). Sample SQ-039 from the Tolombon complex defines a high-T cluster, in line with the 800-850 °C estimated for peak metamorphism in rocks with Opx. Titanites from the Agua del Sapo complex, in contrast, show a broad gentle curve with temperatures consistently above 700 °C over 120 Ma, and reaching 750 °C around 460 Ma. The pattern suggests a gentle prograde heating followed by a slow cooling.

5 Discussion

5.1 The nature of D2

Deformation of the Agua del Sapo complex

D1 structures preserved in lithons in the Agua del Sapo complex have been strongly overprinted by a second set of structures that were not recorded in hanging wall Tolombon complex. The dominant deformation features in the Agua del Sapo complex are: a) intense simple shear deformation with top-to-south kinematics, b) a strong N-S subhorizontal stretching lineation associated with constrictional L-tectonites, parallel to the transport direction of shear zones and the axis of sheath folds, and c) upright N or S-gently plunging folds.

The top-to-south shear sense, independently of the dip of the foliation (e.g., Catalino versus Talapaso Shear Zone in Fig. 11, lower inset), is consistent with upright folding of south-verging thrust shear zones. Thus, the sinistral Filo Shear Zone, marking the westernmost boundary of this sheared terrane, can be interpreted as part of a south-directed thrust that was over-steepened in the limb of a fold, consistent with the observed increase in strain in its vicinity, and marked by the tightening of folds (Fig. 2 lower cross-section). The exact temporal relationship between upright folding and south-directed thrusting is unclear. The two could have developed together, or folding overprinted thrusting. In either case, the two features can be interpreted as part of the same deformation event that achieved vertical and horizontal shortening defining constriction with a N-S stretching (e.g., Fig. 3 in Bons et al., 2016).

The tubular sheath folds indicate constrictional strain within shear zones (Ramsay and Huber, 1983; Sullivan, 2013). Constriction is also suggested by the orientation of long minerals in combination with quartz CPO patterns (Fig. 9)(Sullivan, 2013). This conclusion supports the interpretation that upright folding, S-verging thrusting, N-S stretching and sheath folds, all developed broadly contemporaneously as a result of a non-coaxial constrictional D2 event (Fletcher and Bartley, 1994), with a N-S stretching axis and top-to-south kinematics. This phase stretched the crust parallel to the orogen while translating the Tolombon complex on the hanging wall of the Pichao Shear Zone to the south.

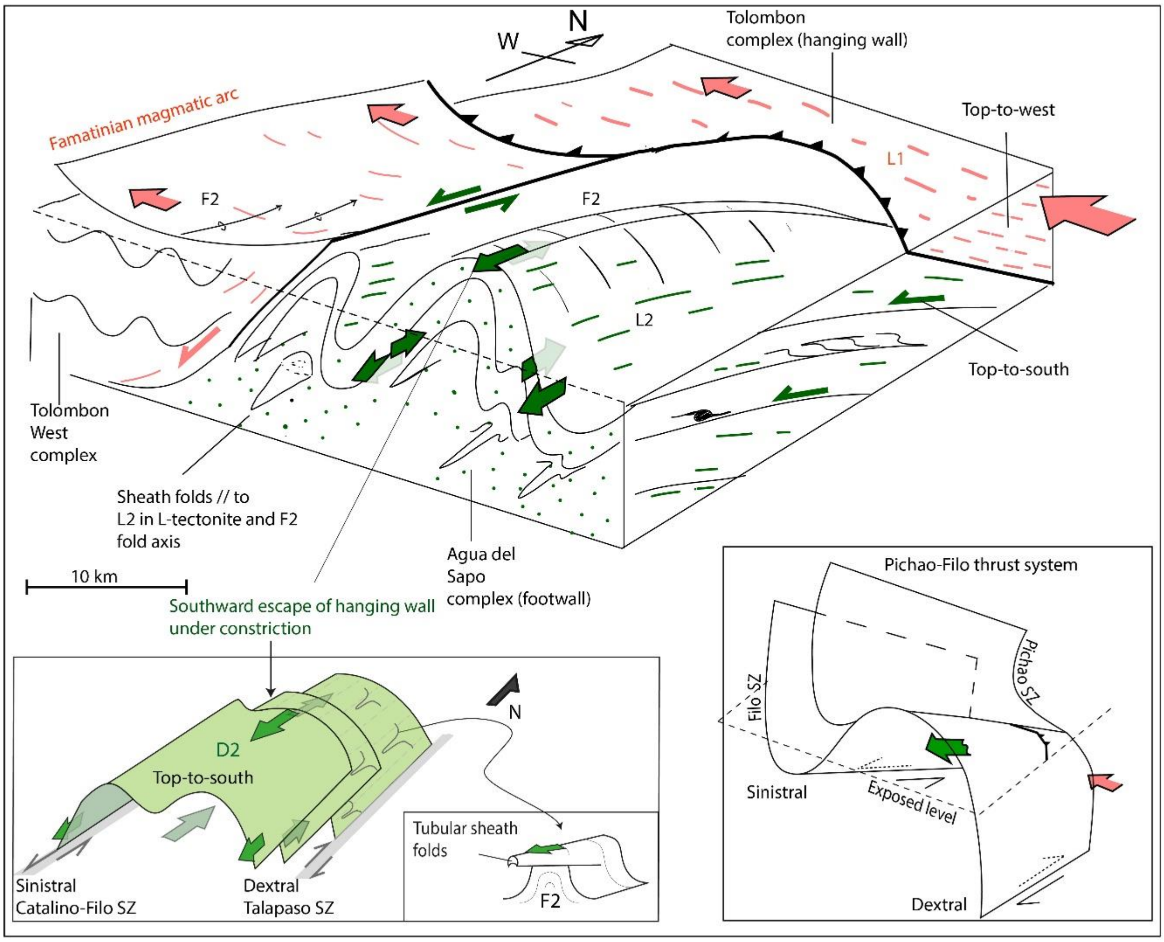

Figure 11. Kinematics of D1 (red arrows) and D2 (green arrows) in the Sierra de Quilmes with details of the Agua del Sapo complex structures. In the Tolombon and Tolombon West complexes west-verging thrusts related to D1 are preserved while in the Agua del Sapo complex D2 dominates. Here, open upright F2 folds with dextral and sinistral shear zones on opposite limbs define a southward tectonic transport (inset in lower left). F2 fold axis is parallel to stretching lineations and L-tectonites indicating a non-coaxial constrictional regime. Inset in lower right corner depicts the geometry of the Pichao-Filo thrust system folded and plunging to the north.

D2 in Tolombon West complex

Unlike the Agua del Sapo complex, D2 in the Tolombon West complex lacks the intense lineation, evidence for constriction, and intense simple shear. D2 is instead expressed mostly as folding with only subordinate shearing, focused on the vicinity of the sinistral Filo Shear Zone. This shear zone defines a broad arc, rotating gradually southwards from N-S striking into smaller splays striking NE-SW, marking the contact with the lower magnetic susceptibility rocks of the Agua del Sapo complex

(Fig. 3). The regional foliation rotates into parallelism with the main trend of the Filo Shear Zone. Also, the syn-anatectic upright F2 folds, varying from metric-scale to 100s of metres, trend parallel to the Filo Shear Zone trace as it rotates. Folds become more intense to the south where they are overprinted by the narrow (5-15 cm wide) sillimanite-bearing dextral shear zones parallel to S2.

We interpret the splaying of the Filo Shear Zone as reflecting the end of the strike-slip shear zone accompanied by movement transfer into the upright folds, that intensify southwards. This movement transfer caused shortening and possibly thrusting of the Tolombon West against the Agua del Sapo complex to the south (Fig. 3). The NE-striking dextral shear zones, parallel to the axial planes in this region of movement transfer developed in the stability field of sillimanite and their kinematics suggest a NNW-SSE-driven transpression partitioned between folds and shear zone, possibly as part of the same D2 event.

We conclude therefore that during D2 the strain ellipsoid must have changed from a prolate N-S ellipsoid in the Agua del Sapo complex, with a strong simple shear component, to an oblate ellipsoid with a maximum shortening oriented E-W in the north of the Tolombon West complex to NNW-SSE in its south, where the influence of the movement transfer from the strike slip shear zone is significant.

5.2 The Pichao-Filo thrust system

The geometric arrangement and similarities between the Filo and Pichao Shear Zones (Fig. 2) suggest they formed an interconnected system: (i) they are both wide mylonite-ultramylonite shear zones, (ii) their strain profile is asymmetric, with sharp strain gradient against the Agua del Sapo complex rocks of the footwall and gradational transition towards the hanging wall, and (iii) they have syn-kinematic sillimanite and dynamically recrystallized quartz and Kfs, suggesting high-grade metamorphic conditions of deformation, weakly overprinted by greenschist facies retrogression (Finch et al., 2015).

We argue that the Filo Shear Zone together with the eastern section of the Pichao Shear Zone form the basal decollement of a thrust system, and the Tolombon West complex is a horse that is bound by the Filo Shear Zone and the western section of the Pichao Shear Zone (Fig. 12). This system, called here the Pichao-Filo thrust system, placed the Tolombon over the Tolombon West complex, and both were thrusted over the Agua del Sapo complex above the basal decollement during D1. Thrusting led to cooling of the hanging wall rocks that is well-constrained to ~450-440 Ma by the youngest zircon group in Wolfram (2019) and the titanite ages from the Tolombon complex (sample SQ-039 analysed here). In contrast the Agua del Sapo complex footwall remained hot to ~380 Ma (Fig. 10) and continued to be intensely deformed by D2.

We envisage that during D2 the basal decollement and the Agua del Sapo footwall were folded upright causing a rotation and steepening of the Filo Shear Zone, as well as its reactivation into a sinistral shear zone, in response to the top-to-south motion (Fig. 12). This reactivation is responsible for the ~7 km sinistral deflection of the Pichao Shear Zone and its overprinting by sub-horizontal stretching lineation in the deflected region. The intense constrictonal D2 deformation in the Agua del Sapo complex is presumably because of strain localization to this region that remained hotter than the hanging wall complexes.

The evolution of the deformation suggests that D1 lithospheric thickening resulting from westward thrusting perpendicular to the orogen became impeded. This could be a result of the orogen reaching a critical thickness where a balance was reached between the east-west maximum compressional stress and the vertical gravitational stress. Under these conditions, continued east-west shortening led to D2 constriction restricted to the warmer footwall complex (Fig. 11). The thrusting to the south during constriction indicates that the lithosphere to the south had not reached the same critical state and that there was still room for thickening allowing for southward lateral escape of the rock mass to fill this gap.

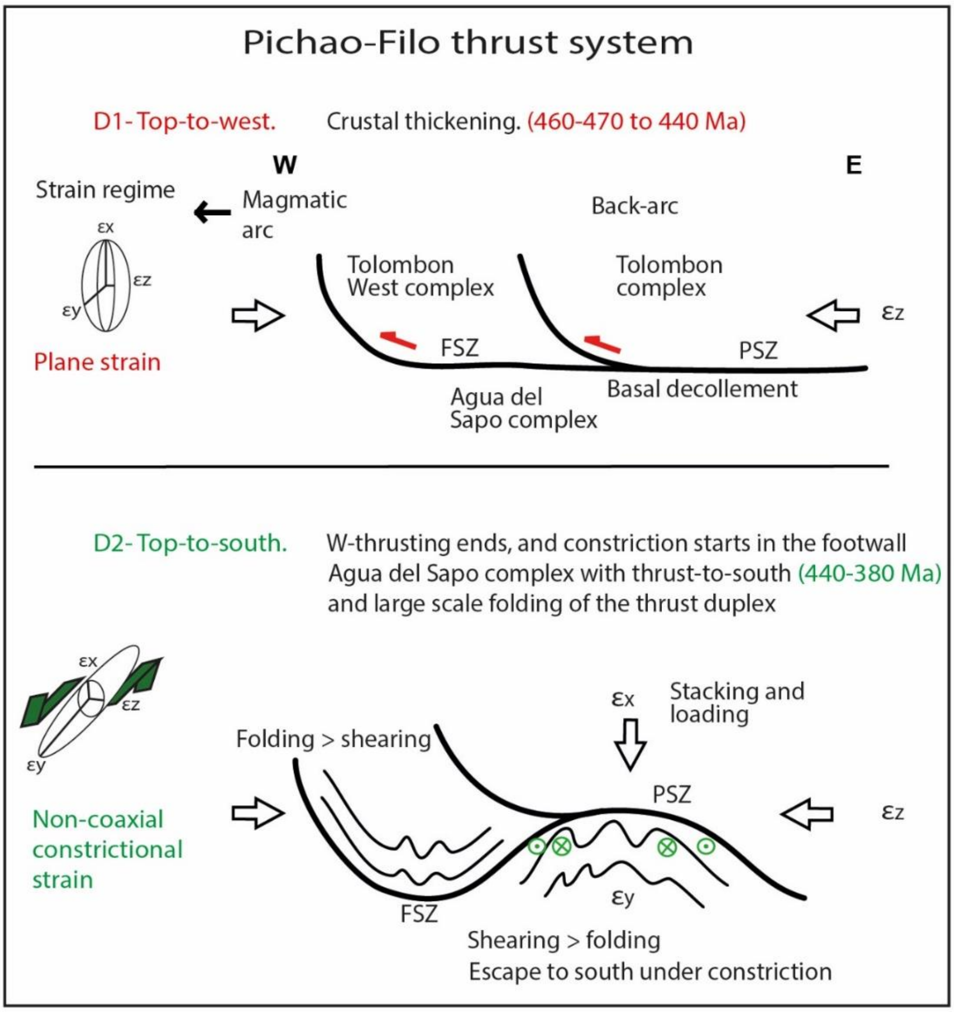

Figure 12. Pichao-Filo thrust system, and interpretation of its evolution on cross sections. First, top-to-west thrusting (D1) thickened the crust and transported rocks to the west, towards the magmatic arc. Thrusting then becomes impeded, and stretching parallel to the orogen in a non-coaxial constrictional regime takes over in the thermally weakened Agua del Sapo complex, accompanied by folding and thrusting to the south (D2). During D2, E-W stresses were counterbalanced by vertical stresses and regional force balances lead to southward thrusting in this new constrictional setting.

5.3 Metamorphic conditions during D1 and D2

D1 was contemporaneous with anatexis in all three metamorphic complexes. In the Tolombon and Tolombon West complexes, anatexis was more voluminous than in the Agua del Sapo complex because of their Al-rich protolith and higer PT conditions. Regardles of that, D1 top-to-west thrusting and folding in Tolombon and Tolombon West complexes were associated with peak metamorphic conditions evidenced by leucosomes that are parallel to the S1 axial planar foliation and shear planes (Figs. 4c and 6a)(Finch et al., 2015; Finch et al., 2016). Similar features are also observed in the Agua del Sapo complex preserved in the lithons.

D2 was also contemporaneous with anatexis in the Tolombon West and Agua del Sapo complexes. In both areas S2 axial planar foliations include biotite and sillimanite (Fig. 4a) and leucosomes are preferentially oriented parallel to S2 (Figs. 4e, 6a, 7c), or in shear zones in the Tolombon West complex. There is also evidence for later undeformed leucosomes cross-cutting deformed metatexites (Fig. 4b, h). Anatexis during D1 and D2 suggests protracted supra-solidus conditions in the Sierra de Quilmes, in accordance with the findings of Wolfram et al. (2019) and further supported by the Zr-in-titanite thermometry (Fig. 10).

In the D2 shear zones of the Agua del Sapo complex, the K-feldspar porphyroclasts with core-and-mantle textures and myrmekite are similar to microstructures reported in granitic mylonites that underwent deformation between 450 and 600 °C (Rosenberg and Stünitz, 2003; Tullis and Yund, 1991). Quartz shows evidence for sub-grain rotation (SGR) that sometimes progress to an oblique foliation, in the combined SGR and GBM recrystallisation regime (Passchier and Trouw, 2005). These features are overprinted by substantial quartz BLG, and quartz ribbons and aggregates also show recovery to polygonal grains lacking undulose extinction. These features form between ~600 °C (GBM-SGR) and ~400 °C (BLG) and indicate cooling during D2. The Agua del Sapo complex underwent intense muscovitization and muscovite blasts now form mica fish. Muscovitization occurred in both the Agua del Sapo and Tolombon West where D2 has been recorded, but is absent in the Tolombon complex that lacks clear signs of D2. We argue therefore that D2 must have evolved from the higher end of amphibolite facies associated with local anatexis, to the lower end of amphibolite facies with pervasive fluid influx and muscovitization. Muscovitization of the Tolombon West complex gave rise to centimetric grains that are randomly oriented suggesting a late tectonic growth.

Metamorphic conditions of the Filo Shear Zone

The Filo Shear Zone and its splays in the Tolombon West complex preserve grain boundary migration (GBM) in quartz (Fig. 6d), suggesting temperatures above 500 °C (Stipp et al., 2002). This recrystallised quartz have grain-sizes ranging between ~200-400 µm, which is common in mylonite developed at temperatures > 650 °C (Rosenberg and Handy, 2005; Rosenberg and Stünitz, 2003) or >

~550 °C (Stipp et al., 2002). The coexistence of quartz GBM and bulging (BLG) in the same sample (Fig. 6e), suggest also shearing at lower temperatures (~400 °C, Stipp et al., 2002). These temperatures only provide broad constraints as the recrystallisation mechanism is strongly influenced by the presence of fluids, differential stress, and variable strain rate (Law, 2014; Passchier and Trouw, 2005). Better constraints are provided by the stable paragenesis. This includes syn-kinematic sillimanite suggesting shearing at upper amphibolite facies conditions (Büttner et al., 2005; Larrovere et al., 2008), while the presence of epidote with allanite cores in Ca-rich mylonitic rocks are stable below 700-750 °C (Budzyń et al., 2017; Janots et al., 2008; Wing et al., 2003). Combining quartz microstructures and mineral paragenesis, we estimate that the Filo Shear Zone developed at amphibolite facies conditions with temperatures between 700 and 550 °C, and was overprinted at ~400 °C as evidenced by the BLG of quartz and weak chloritization of the stable mineralogy. The latter was probably a low-intensity deformation, insufficient to erase the GBM features.

5.4 Timing of D2

Titanite dates in the Tolombon complex, between 475-440 Ma (Fig. 10a) compare with monazite and zircon dates between ~505-440 Ma (Finch et al., 2017; Weinberg et al., 2020; Wolfram et al., 2019). All three geochronometres closed their isotopic systems at ~440 Ma, inferred to date the cooling resulting from exhumation related to D1 thrusting (Finch et al., 2017). Given that shortening in the Famatinian orogeny started between 470 to 460 Ma (Weinberg et al., 2019), it is likely that D1 took place between 470-460 Ma and ~440 Ma.

Unlike the Tolombon complex, the Agua del Sapo complex remained hot for longer (Fig. 10). Finch et al. (2017) reported monazite U-Pb ages from two samples from the Agua del Sapo complex. Monazite from a schist in the immediate footwall of the PSZ (SQ84a) yielded dates that range between 490-450 Ma, similar to those of the hanging wall. The other sample, from ~1 km further south (SQ181a), yielded dates between 435-420 Ma. These two date groups are reflected in our titanite dates in Fig. 10, with some samples yielding dates between ~500 and 440 Ma, and others between ~440 and ~380 Ma.

The entire 120 Ma range recorded by titanite in the Agua del Sapo complex, from 500 to 380 Ma, is associated with Zr-in-titanite temperatures between ~750-700 °C, peaking at ~460 Ma and cooling gently thereafter (Fig. 10b). This suggests that the footwall of the Pichao-Filo thrusts remained at or above 700 °C some 60 Ma longer than the hanging wall, undergoing a very slow cooling during this period, at rates of ~1 °C/Ma. The growth of monazite and titanite in the footwall after 440 Ma was likely assisted by both sustained high temperatures and shearing. Lucassen (2003) reported a similar case to the west of the Sierra de Quilmes, in another Famatinian migmatitic terrane, where deformation-enhanced recrystallization of titanite at temperature > 650 ^{o}C resulted in a semi-continuous titanite formation between 470-420 Ma (see also (Gasser et al., 2015) for protracted titanite formation). A remaining question is why did titanite from different samples record different periods of the metamorphic history when the samples have similar mineralogical and structural makeup? The answer could be related to different mineral reactivity related to small compositional differences between samples, or variable distribution of deformation and/or fluids (Cherniak et al., 2004; Harlov and Hetherington, 2010; Schoene, 2014; Taylor et al., 2016).

5.5 Sustained high-temperatures and the origin of D2

Back-arc terranes, such as that of the Famatinian Orogen, are wide, hot and rheologically weak parts of the crust (Hyndman et al., 2005). They are therefore susceptible to take up deformation. During shortening, back-arcs may be too weak to build up a thick crust and are instead prone to lateral and transversal spread (Beaumont et al., 2010; Cruden et al., 2006; Jamieson and Beaumont, 2013) maintaining a subdued topography. The magnitude of this flow depends on the balance between crustal thickening and gravity-driven extension (Jamieson et al., 2011), and modulated by partial melting (Vanderhaeghe, 2009; Vanderhaeghe and Teyssier, 2001). Hot orogens where lateral flow leads to a subdued topography will form plateaus underlain by a weak ductile crust. A classic example of this is the thermally softened Variscan orogen that Franke et al. (2014) described as a “failed” orogen, unfit for stacking.

The protracted high-temperature conditions in Sierra de Quilmes with evidence for multiple melting events (Wolfram et al., 2019), suggests that heat was inherited from the early extensional phase that lasted from ca. 500 to 470-460 Ma (Weinberg et al., 2018), and sustained long-term by a combination of modest crustal thickening of a heat producing crust and intense heat flow from the mantle (Wolfram et al., 2017). The switch at 470-460 Ma, from extension to the shortening phase started the Oclóyic phase resulting in both D1 and D2 events.

In summary, the Sierra de Quilmes exposes the mid-crustal section of the thermally-mature Famatinian continental back-arc that during the Oclóyic phase evolved from a stage of thickening (D1), where the three HT-LP complexes were stacked forming a large thrust duplex, to a stage of southward thrusting and N-S stretching (D2). D1 lasted from 470-460 Ma and ended at ~440 Ma when thrust-to-west was impeded and D2 started. The colder hanging wall complexes were little affected by D2, with only folding and minor shearing recorded in the Tolombon West complex. Intense deformation with constriction and top-to-south thrusting was restricted to the hot Agua del Sapo footwall. D2 can be explained by a regional imbalance of the vertical forces that caused a lateral pressure gradient. We postulate that lithospheric thickening during D1 was more intense to the north driving material escape to the south during D2.

6 Conclusion

The Sierra de Quilmes records two major deformational events that occurred during the shortening Oclóyic phase of the Famatinian orogenic cycle. The first event, D1, is characterised by a high-temperature syn-anatectic thrust-to-the-west, forming the Pichao-Filo thrust system and a large-scale duplex structure. Lithospheric thickening as a result of D1 reached a critical point in which further thrusting was impeded. At this point D2 started, characeterized by constriction with a N-S stretching direction, and N-S doubly plunging folds and thrusting to the south, parallel to the orogen. While this event did not affect the hanging wall Tolombon complex, it led to syn-anatectic folding in the Tolombon West complex, and intense, syn-anatectic shearing in the Agua del Sapo complex, the footwall of the duplex. The latter was strongly stretched, folded and thrusted in this non-coaxial constrictional event. The deformation history was therefore characterized by a continuous, unidirectional east-west convergence that evolved from thrusting perpendicular to the orogen from 470-460 to ~440 Ma, to thrusting parallel to the orogen thereafter, driven by lateral variations in lithospheric thicknesses. Titanite geochronology and geothermometry suggest that the footwall remained hot and structurally active between ~440 possibly to 380 Ma, long after the hanging wall had cooled and ceased deforming. In summary, the Oclóyic phase of the Famatinian orogen gave rise to a long-lived, wide and hot orogen that was too weak to sustain high topography, forcing the orogenic edifice to spread laterally similar to the thermally weakened Grenvillian or Variscan orogens (Beaumont et al., 2010; Jamieson and Beaumont, 2013), and the mid-crustal sections of the Himalayan (Parsons et al., 2016).

Acknowledgements

We thank David Kelsey for the comments and discussion that improved significantly this manuscript. We thank also colleagues49 from the Universidad de Salta, Nestor Suzaño, Agustin Ortiz and Alexis Nieves for the discussions and support in the extraordinary field trips. This research was supported by the Australian Research Council grant no. DP110102543 (to R.F.W.).

Datasets for this research are available at Monash University repository: https://figshare.com/s/5ed9fc54d98be2e32ff2

References

Aceñolaza, F. G., Miller, H., and Toselli, A. J., 2002, Proterozoic - Early Paleozoic evolution in western South America - A discussion: Tectonophysics, v. 354, p. 121-137.

Adams, C. J., Miller, H., Aceñolaza, F. G., Toselli, A. J., and Griffin, W. L., 2011, The Pacific Gondwana margin in the late Neoproterozoic–early Paleozoic: Detrital zircon U–Pb ages from metasediments in northwest Argentina reveal their maximum age, provenance and tectonic setting: Gondwana Research, v. 19, p. 71-83.

Aleinikoff, J. N., Wintsch, R. P., Tollo, R. P., Unruh, D. M., Fanning, C. M., and Schmitz, M. D., 2007, Ages and origins of rocks of the Killingworth dome, south-central Connecticut: Implications for the tectonic evolution of southern New England: American Journal of Science, v. 307, p. 63-118.

Astini, R., 2008, Sedimentación, facies, discordancias y evolución paleoambiental durante el Cambro-Ordovícico, Revista de la Asociacion Geologica Argentina, 50-73 p.

Astini, R. A., 1998, Stratigraphical evidence supporting the rifting, drifting and collision of the Laurentian Precordillera terrane of western Argentina, The Geological Society, v. 142, p. 11-33.

Astini, R. A., and Dávila, F. M., 2004, Ordovician back arc foreland and Ocloyic thrust belt development on the western Gondwana margin as a response to Precordillera terrane accretion: Tectonics, v. 23, p. TC4008 1-19.

Bahlburg, H., Berndt, J., and Gerdes, A., 2016, The ages and tectonic setting of the Faja Eruptiva de la Puna Oriental, Ordovician, NW Argentina: Lithos, v. 256-257, p. 41-54.

Bahlburg, H., and Breitkreuz, C., 1991, Paleozoic evolution of active margin basins in the southern Central Andes (northwestern Argentina and northern Chile): Journal of South American Earth Sciences, v. 4, p. 171-188.

Bahlburg, H., and Hervé, F., 1997a, Geodynamic evolution and tectonostratigraphic terranes of northwestern Argentina and northern Chile: Bulletin of the Geological Society of America, v. 109, p. 869-884.

Bahlburg, H., and Hervé, F., 1997b, Geodynamic evolution and tectonostratigraphic terranes of northwestern Argentina and northern Chile: Geological Society of America Bulletin, v. 109, p. 869-884.

Beaumont, C., Jamieson, R., and Nguyen, M., 2010, Models of large, hot orogens containing a collage of reworked and accreted terranes: Canadian Journal of Earth Sciences, v. 47, p. 485-515.

Bons, P. D., Jansen, D., Mundel, F., Bauer, C. C., Binder, T., Eisen, O., Jessell, M. W., Llorens, M. G., Steinbach, F., Steinhage, D., and Weikusat, I., 2016, Converging flow and anisotropy cause large-scale folding in Greenland's ice sheet: Nature Communications, v. 7.

Braathen, A., Nordgulen, O., Osmundsen, P. T., Andersen, T. B., Solli, A., and Roberts, D., 2000, Devonian, orogen-parallel, opposed extension in the Central Norwegian Caledonides: Geology, v. 28, p. 615-618.

Budzyń, B., Harlov, D. E., Kozub-Budzyń, G. A., and Majka, J., 2017, Experimental constraints on the relative stabilities of the two systems monazite-(Ce) – allanite-(Ce) – fluorapatite and xenotime-(Y) – (Y,HREE)-rich epidote – (Y,HREE)-rich fluorapatite, in high Ca and Na-Ca environments under P-T conditions of 200–1000 MPa and 450–750 °C: Mineralogy and Petrology, v. 111, p. 183-217.

Büttner, S. H., 2009, The Ordovician Sierras Pampeanas–Puna basin connection: Basement thinning and basin formation in the Proto-Andean back-arc: Tectonophysics, v. 477, p. 278-291.

Büttner, S. H., Glodny, J., Lucassen, F., Wemmer, K., Erdmann, S., Handler, R., and Franz, G., 2005, Ordovician metamorphism and plutonism in the Sierra de Quilmes metamorphic complex: Implications for the tectonic setting of the northern Sierras Pampeanas (NW Argentina): Lithos, v. 83, p. 143-181.

Carreras, J., Cosgrove, J. W., and Druguet, E., 2013, Strain partitioning in banded and/or anisotropic rocks: Implications for inferring tectonic regimes: Journal of Structural Geology, v. 50, p. 7-21.

Cawood, P. A., 2005, Terra Australis Orogen: Rodinia breakup and development of the Pacific and Iapetus margins of Gondwana during the Neoproterozoic and Paleozoic: Earth-Science Reviews, v. 69, p. 249-279.

Chambers, J. A., and Kohn, M. J., 2012, Titanium in muscovite, biotite, and hornblende: Modeling, thermometry, and rutile activities of metapelites and amphibolites: American Mineralogist, v. 97, p. 543-555.

Chardon, D., Gapais, D., and Cagnard, F., 2009, Flow of ultra-hot orogens: A view from the Precambrian, clues for the Phanerozoic: Tectonophysics, v. 477, p. 105-118.

Chardon, D., and Jayananda, M., 2008, Three-dimensional field perspective on deformation, flow, and growth of the lower continental crust (Dharwar craton, India): Tectonics, v. 27.

Chardon, D., Jayananda, M., and Peucat, J.-J., 2011, Lateral constrictional flow of hot orogenic crust: Insights from the Neoarchean of south India, geological and geophysical implications for orogenic plateaux: Geochemistry Geophysics Geosystems - GEOCHEM GEOPHYS GEOSYST, v. 12.

Cherniak, D. J., Watson, E. B., Grove, M., and Harrison, T. M., 2004, Pb diffusion in monazite: A combined RBS/SIMS study: Geochimica et Cosmochimica Acta, v. 68, p. 829-840.

Collins, W. J., 2002, Hot orogens, tectonic switching, and creation of continental crust: Geology, v. 30, p. 535-538.

Cruden, A. R., Nasseri, M. H. B., and Pysklywec, R., 2006, Surface topography and internal strain variation in wide hot orogens from three-dimensional analogue and two-dimensional numerical vice models, Geological Society Special Publication, 253, p. 79-104.

Currie, C. A., and Hyndman, R. D., 2006, The thermal structure of subduction zone back arcs: Journal of Geophysical Research: Solid Earth, v. 111.

Davila, F. M., Astini, R. A., and Schmidt, C. J., 2003, Unraveling 470 m.y. of shortening in the Central Andes and documentation of Type O superposed folding: Geology, v. 31, p. 275-278.

Escayola, M. P., van Staal, C. R., and Davis, W. J., 2011, The age and tectonic setting of the Puncoviscana Formation in northwestern Argentina: An accretionary complex related to Early Cambrian closure of the Puncoviscana Ocean and accretion of the Arequipa-Antofalla block: Journal of South American Earth Sciences, v. 32, p. 438-459.

Finch, M. A., Weinberg, R. F., Fuentes, M. G., Hasalová, P., and Becchio, R., 2015, One kilometre-thick ultramylonite, Sierra de Quilmes, Sierras Pampeanas, NW Argentina: Journal of Structural Geology, v. 72, p. 33-54.

Finch, M. A., Weinberg, R. F., Hasalová, P., Becchio, R., Fuentes, M. G., and Kennedy, A., 2017, Tectono-metamorphic evolution of a convergent back-arc: The Famatinian orogen, Sierra de

Quilmes, Sierras Pampeanas, NW Argentina: Bulletin of the Geological Society of America, v. 129, p. 1602–1621.

Finch, M. A., Weinberg, R. F., and Hunter, N. J. R., 2016, Water loss and the origin of thick ultramylonites: Geology, v. 44, p. 599-602.

Fletcher, J. M., and Bartley, J. M., 1994, Constrictional strain in a non-coaxial shear zone: implications for fold and rock fabric development, central mojave metamorphic core complex, california: Journal of Structural Geology, v. 16, p. 555-570.

Franke, W., 2014, Topography of the Variscan orogen in Europe: Failed-not collapsed: International Journal of Earth Sciences, v. 103, p. 1471-1499.

Gasser, D., Jeřábek, P., Faber, C., Stünitz, H., Menegon, L., Corfu, F., Erambert, M., and Whitehouse, M. J., 2015, Behaviour of geochronometers and timing of metamorphic reactions during deformation at lower crustal conditions: Phase equilibrium modelling and U-Pb dating of zircon, monazite, rutile and titanite from the Kalak Nappe Complex, northern Norway: Journal of Metamorphic Geology, v. 33, p. 513-534.

Hajná, J., Žák, J., Kachlík, V., and Chadima, M., 2012, Deciphering the Variscan tectonothermal overprint and deformation partitioning in the Cadomian basement of the Teplá-Barrandian unit, Bohemian Massif: International Journal of Earth Sciences, v. 101, p. 1855-1873.

Harlov, D. E., and Hetherington, C. J., 2010, Partial high-grade alteration of monazite using alkali-bearing fluids: Experiment and nature: American Mineralogist, v. 95, p. 1105-1108.

Hayden, L. A., Watson, E. B., and Wark, D. A., 2008, A thermobarometer for sphene (titanite): Contributions to Mineralogy and Petrology, v. 155, p. 529-540.

Heilbronner, R., and Tullis, J., 2006, Evolution of c axis pole figures and grain size during dynamic recrystallization: Results from experimentally sheared quartzite: Journal of Geophysical Research: Solid Earth, v. 111.

Heuret, A., Funiciello, F., Faccenna, C., and Lallemand, S., 2007, Plate kinematics, slab shape and back-arc stress: A comparison between laboratory models and current subduction zones: Earth and Planetary Science Letters, v. 256, p. 473-483.

Heuret, A., and Lallemand, S., 2005, Plate motions, slab dynamics and back-arc deformation: Physics of the Earth and Planetary Interiors, v. 149, p. 31-51.

Horstwood, M. S. A., Košler, J., Gehrels, G., Jackson, S. E., McLean, N. M., Paton, C., Pearson, N. J., Sircombe, K., Sylvester, P., Vermeesch, P., Bowring, J. F., Condon, D. J., and Schoene, B., 2016, Community-Derived Standards for LA-ICP-MS U-(Th-)Pb Geochronology – Uncertainty Propagation, Age Interpretation and Data Reporting: Geostandards and Geoanalytical Research, v. 40, p. 311-332.

Hunter, N. J. R., Hasalová, P., Weinberg, R. F., and Wilson, C. J. L., 2016, Fabric controls on strain accommodation in naturally deformed mylonites: The influence of interconnected micaceous layers: Journal of Structural Geology, v. 83, p. 180-193.

Hyndman, R. D., Currie, C. A., and Mazzotti, S. P., 2005, Subduction zone backarcs, mobile belts, and orogenic heat: GSA Today, v. 15, p. 4-10.

Jamieson, R. A., and Beaumont, C., 2013, On the origin of orogens: Bulletin of the Geological Society of America, v. 125, p. 1671-1702.

Jamieson, R. A., Unsworth, M. J., Harris, N. B. W., Rosenberg, C. L., and Schulmann, K., 2011, Crustal melting and the flow of mountains: Elements, v. 7, p. 253-260.

Janots, E., Engi, M., Berger, A., Allaz, J., Schwarz, J. O., and Spandler, C., 2008, Prograde metamorphic sequence of REE minerals in pelitic rocks of the Central Alps: Implications for allanite-monazite-xenotime phase relations from 250 to 610°C: Journal of Metamorphic Geology, v. 26, p. 509-526.

Jolivet, L., Famin, V., Mehl, C., Parra, T., Aubourg, C., Hébert, R., and Philippot, P., 2004, Strain localization during crustal-scale boudinage to form extensional metamorphic domes in the Aegean Sea: Geological Society of America Spetial Paper 380, p. 185-210.

Kapp, P., Manning, C. E., and Tropper, P., 2009, Phase-equilibrium constraints on titanite and rutile activities in mafic epidote amphibolites and geobarometry using titanite-rutile equilibria: Journal of Metamorphic Geology, v. 27, p. 509-521.

Kennedy, A. K., Kamo, S. L., Nasdala, L., and Timms, N. E., 2010, Grenville skarn titanite: Potential reference material for sims U-Th-Pb analysis: Canadian Mineralogist, v. 48, p. 1423-1443.

Kilian, R., Heilbronner, R., and Stünitz, H., 2011, Quartz grain size reduction in a granitoid rock and the transition from dislocation to diffusion creep: Journal of Structural Geology, v. 33, p. 1265-1284.

Kohn, M. J., 2017, Titanite Petrochronology: Reviews in Mineralogy and Geochemistry, v. 83, p. 419-441.

Larrovere, M. A., Alasino, P. H., and Baldo, E. G., 2016, The double-vergent ductile shear zone of northwestern sierra de Velasco: Deformation of the middle crust during the Famatinian orogeny: Revista de la Asociacion Geologica Argentina, v. 73, p. 117-133.

Larrovere, M. A., de los Hoyos, C. R., Toselli, A. J., Rossi, J. N., Basei, M. A. S., and Belmar, M. E., 2011, High T/P evolution and metamorphic ages of the migmatitic basement of northern Sierras Pampeanas, Argentina: Characterization of a mid-crustal segment of the Famatinian belt: Journal of South American Earth Sciences, v. 31, p. 279-297.

Larrovere, M. A., Toselli, A., and Rossi De Toselli, J. N., 2008, Petrology and structure of La Chilca Shear Zone, Catamarca: Revista de la Asociacion Geologica Argentina, v. 63, p. 254-263.

Law, R. D., 2014, Deformation thermometry based on quartz c-axis fabrics and recrystallization microstructures: A review: Journal of Structural Geology, v. 66, p. 129-161.

Lister, G., and Forster, M., 2009, Tectonic mode switches and the nature of orogenesis: Lithos, v. 113, p. 274-291.

Lister, G. S., and Hobbs, B. E., 1980, The simulation of fabric development during plastic deformation and its application to quartzite: the influence of deformation history: Journal of Structural Geology, v. 2, p. 355-370.

Lucassen, F., and Becchio, R., 2003, Timing of high-grade metamorphism: Early Palaeozoic U-Pb formation ages of titanite indicate long-standing high-T conditions at the western margin of Gondwana (Argentina, 26-29°S): Journal of Metamorphic Geology, v. 21, p. 649-662.

Malavieille, J., 1993, Late Orogenic extension in mountain belts: Insights from the basin and range and the Late Paleozoic Variscan Belt: Tectonics, v. 12, p. 1115-1130.

Mancktelow, N. S., and Pavlis, T. L., 1994, Fold-fault relationships in low-angle detachment systems: Tectonics, v. 13, p. 668-685.

Moya, M., 2015, La Fase Ocloyica (Ordovicico Superior) en el noroeste argentino. Interpretacion historica y evidencias en contrario: Serie Correlacion Geologica, v. 3, p. 73-110.

Mulcahy, S. R., Roeske, S. M., McClelland, W. C., Ellis, J. R., Jourdan, F., Renne, P. R., Vervoort, J. D., and Vujovich, G. I., 2014, Multiple migmatite events and cooling from granulite facies metamorphism within the Famatina arc margin of northwest Argentina: Tectonics, v. 33, p. 1-25.

Omarini, R. H., Sureda, R. J., Götze, H. J., Seilacher, A., and Pflüger, F., 1999, Puncoviscana folded belt in northwestern Argentina: Testimony of Late Proterozoic Rodinia fragmentation and pre-Gondwana collisional episodes: International Journal of Earth Sciences, v. 88, p. 76-97.

Ortiz, A., Suzaño, N., Hauser, N., Becchio, R., and Nieves, A., 2019, New hints on the evolution of the Eastern Magmatic Belt, Puna Argentina. SW Gondwana margin: Zircon U-Pb ages and Hf isotopes in the Pachamama Igneous-Metamorphic Complex: Journal of South American Earth Sciences, v. 94, p. 102246.

Parsons, A. J., Ferré, E. C., Law, R. D., Lloyd, G. E., Phillips, R. J., and Searle, M. P., 2016, Orogen-parallel deformation of the Himalayan midcrust: Insights from structural and magnetic fabric analyses of the Greater Himalayan Sequence, Annapurna-Dhaulagiri Himalaya, central Nepal: Tectonics, v. 35, p. 2515-2537.

Passchier, C. W., and Trouw, R. A. J., 2005, Microtectonics, Springer Berlin Heidelberg, 1-366 p.

Pennacchioni, G., Menegon, L., Leiss, B., Nestola, F., and Bromiley, G., 2010, Development of crystallographic preferred orientation and microstructure during plastic deformation of natural coarse-grained quartz veins: Journal of Geophysical Research: Solid Earth, v. 115.

Peternell, M., Hasalová, P., Wilson, C. J. L., Piazolo, S., and Schulmann, K., 2010, Evaluating quartz crystallographic preferred orientations and the role of deformation partitioning using EBSD and fabric analyser techniques: Journal of Structural Geology, v. 32, p. 803-817.

Piñán-Llamas, A., and Simpson, C., 2009, Primary structure influence on compositional banding in psammites: Examples from the Puncoviscana Formation, north-central Argentina: Journal of Structural Geology, v. 31, p. 55-71.

Ramos, V. A., 2008, The basement of the Central Andes: The arequipa and related terranes, *in* Jeanloz, R., Albee, A. L., Burke, K. C., and Freeman, K. H., eds., Annual Review of Earth and Planetary Sciences, 36, p. 289-324.

Ramos, V. A., 2009, Anatomy and global context of the Andes: Main geologic features and the Andean orogenic cycle, Memoir of the Geological Society of America, 204, p. 31-65.

Ramos, V. A., Dallmeyer, R. D., and Vujovich, G., 1998, Time constraints on the Early Palaeozoic docking of the Precordillera, central Argentina, Geological Society Special Publication, 142, p. 143-158.

Ramos, V. A., Escayola, M., Mutti, D. I., and Vujovich, G. I., 2000, Proterozoic-early Paleozoic ophiolites of the Andean basement of southern South America, Special Paper of the Geological Society of America, 349, p. 331-349.

Ramos, V. A., Jordan, T. E., Allmendinger, R. W., Mpodozis, C., Kay, S. M., Cortés, J. M., and Palma, M., 1986, Paleozoic terranes of the central Argentine-Chilean Andes: Tectonics, v. 5, p. 855-880.

Ramsay, J. G., and Huber, M. I., 1983, The techniques of modern structural geology. Volume 1: strain analysis: The techniques of modern structural geology. Volume 1: strain analysis.

Rapela, C., Pankhurst, R., Casquet, C., A. Dahlquist, J., Mark Fanning, C., G. Baldo, E., Galindo, C., Alasino, P., Ramacciotti, C., Verdecchia, S., Murra, J., and Basei, M., 2018, A review of the Famatinian Ordovician magmatism in southern South America: Evidence of lithosphere reworking and continental subduction in the early proto-Andean margin of Gondwana: Earth-Science Reviews, v. 187, p. 259-285.

Rapela, C. W., 1976, El Basamento Metamorfico de la Region de Cafayate, Provincia de Salta. Aspectos Petrologicos y Geoquimicos: Revista de la Asociacion Geologica Argentina, v. 3, p. 203-222.

Rapela, C. W., Pankhurst, R. J., Casquet, C., Baldo, E., Saavedra, J., Galindo, C., and Fanning, C. M., 1998a, The Pampean Orogeny of the southern proto-Andes: Cambrian continental collision in the Sierras de Cordoba: Geological Society, London, Special Publications, v. 142, p. 181-217.

Rapela, C. W., Pankhurst, R. J., Saavedra, J., and Galindo, C., 1998b, Early evolution of the proto-andean margin of South America: Geology, v. 26, p. 707-710.

Rapela, C. W., Verdecchia, S. O., Casquet, C., Pankhurst, R. J., Baldo, E. G., Galindo, C., Murra, J. A., Dahlquist, J. A., and Fanning, C. M., 2015, Identifying Laurentian and SW Gondwana sources in the Neoproterozoic to Early Paleozoic metasedimentary rocks of the Sierras Pampeanas: Paleogeographic and tectonic implications: Gondwana Research, v. 32, p. 193-212.

Rosenberg, C. L., and Handy, M. R., 2005, Experimental deformation of partially melted granite revisited: Implications for the continental crust: Journal of Metamorphic Geology, v. 23, p. 19-28.

Rosenberg, C. L., and Stünitz, H., 2003, Deformation and recrystallization of plagioclase along a temperature gradient: An example from the Bergell tonalite: Journal of Structural Geology, v. 25, p. 389-408.

Rossi, J., and Toselli, A., 1976, Migmatization y Metamorfismo en el basamento de la Sierra de Quilmes, al Oeste de Colalao del Valle, Tucuman: Revista de la Asociacion Geologica Argentina, v. 2, p. 83-94.

Rubio Pascual, F. J., López-Carmona, A., and Arenas, R., 2016, Thickening vs. extension in the Variscan belt: P–T modelling in the Central Iberian autochthon: Tectonophysics, v. 681, p. 144-158.

Sawyer, E. W., 2008, Atlas of Migmatites, NRC Research Press and Mineralogical Association of Canada, 387 p.

Schoene, B., 2014, 4.10 - U–Th–Pb Geochronology, *in* Holland, H. D., and Turekian, K. K., eds., Treatise on Geochemistry (Second Edition): Oxford, Elsevier, p. 341-378.

Schoene, B., Condon, D. J., Morgan, L., and McLean, N., 2013, Precision and accuracy in geochronology: Elements, v. 9, p. 19-24.

Schwartz, J. J., Gromet, L. P., and Miro, R., 2008, Timing and Duration of the Calc-Alkaline Arc of the Pampean Orogeny: Implications for the Late Neoproterozoic to Cambrian Evolution of Western Gondwana: The Journal of Geology, v. 116, p. 39-61.

Semenov, I., Weinberg, R., Taylor, R., and Jourdan, F., 2019, Prolonged Movement on a > 10-km-Wide Thrust During Early Paleozoic Orogens in the Gondwana Margin of NW Argentina: Tectonics.

Semenov, I., and Weinberg, R. F., 2017, A major mid-crustal decollement of the Paleozoic convergent margin of western Gondwana: The Guacha Corral shear zone, Argentina: Journal of Structural Geology, v. 103, p. 75-99.

Skjernaa, L., 1989, Tubular folds and sheath folds: definitions and conceptual models for their development, with examples from the Grapesvare area, northern Sweden: Journal of Structural Geology, v. 11, p. 689-703.

Sola, A. M., Becchio, R. A., and Pimentel, M. M., 2013, Petrogenesis of migmatites and leucogranites from Sierra de Molinos, Salta, Northwest Argentina: A petrologic and geochemical study: Lithos, v. 177, p. 470-491.

Sola, A. M., Hasalová, P., Weinberg, R. F., Suzaño, N. O., Becchio, R. A., Hongn, F. D., and Botelho, N., 2017, Low-P melting of metapelitic rocks and the role of H2O: Insights from phase equilibria modelling: Journal of Metamorphic Geology, v. 35, p. 1131-1159.

Stacey, J. S., and Kramers, J., 1975, Approximation of Terrestrial Lead Isotope Evolution by a 2-Stage Model: Earth and Planetary Science Letters, v. 26, p. 207-221.

Stipp, M., Stünitz, H., Heilbronner, R., and Schmid, S. M., 2002, The eastern Tonale fault zone: A 'natural laboratory' for crystal plastic deformation of quartz over a temperature range from 250 to 700 °C: Journal of Structural Geology, v. 24, p. 1861-1884.

Sullivan, W. A., 2009, Kinematic significance of L tectonites in the footwall of a major terrane-bounding thrust fault, Klamath Mountains, California, USA: Journal of Structural Geology, v. 31, p. 1197-1211.

Sullivan, W. A., 2013, L tectonites: Journal of Structural Geology, v. 50, p. 161-175.

Sullivan, W. A., and Beane, R. J., 2010, Asymmetrical quartz crystallographic fabrics formed during constrictional deformation: Journal of Structural Geology, v. 32, p. 1430-1443.

Sullivan, W. A., and Law, R. D., 2007, Deformation path partitioning within the transpressional White Mountain shear zone, California and Nevada: Journal of Structural Geology, v. 29, p. 583-599.

Taylor, R. J. M., Kirkland, C. L., and Clark, C., 2016, Accessories after the facts: Constraining the timing, duration and conditions of high-temperature metamorphic processes: Lithos, v. 264, p. 239-257.

Thomas, W. A., and Astini, R. A., 2003, Ordovician accretion of the Argentine Precordillera terrane to Gondwana: A review: Journal of South American Earth Sciences, v. 16, p. 67-79.

Toselli, A., Rossi, J., and Rapela, C. W., 1978, El Basamento Metamorfico de la Sierra de Quilmes, Republica Argentina: Revista de la Asociacion Geologica Argentina, v. 33, p. 105-121.

Tullis, J., and Yund, R. A., 1991, Diffusion creep in feldspar aggregates: experimental evidence: Journal of Structural Geology, v. 13, p. 987-1000.

Turner, J. C. M., 1975, Geología del sector oriental de los Departamentos de Santa Victoria e Iruya, Provincia de Salta. República Argentina: Boletín de la Academia Nacional de Ciencias: Boletín de la Academia Nacional de Ciencias, v. 51, p. 11-24.

Vanderhaeghe, O., 2009, Migmatites, granites and orogeny: Flow modes of partially-molten rocks and magmas associated with melt/solid segregation in orogenic belts: Tectonophysics, v. 477, p. 119-134.

Vanderhaeghe, O., and Teyssier, C., 2001, Partial melting and flow of orogens: Tectonophysics, v. 342, p. 451-472.

Weinberg, R. F., Becchio, R., Farias, P., Suzaño, N., and Sola, A., 2018b, Early Paleozoic accretionary orogenies in NW Argentina: Growth of West Gondwana: Earth-Science Reviews, v. 187, p. 219-247.

Weinberg, R. F., Wolfram, L. C., Nebel, O., Hasalová, P., Závada, P., Kylander-Clark, A. R. C., and Becchio, R., 2020, Decoupled U-Pb date and chemical zonation of monazite in migmatites: The case for disturbance of isotopic systematics by coupled dissolution-reprecipitation: Geochimica et Cosmochimica Acta, v. 269, p. 398-412.

Whitney, D. L., and Evans, B. W., 2010, Abbreviations for names of rock-forming minerals: American Mineralogist, v. 95, p. 185-187.

Wilson, C. J. L., Russell-Head, D. S., Kunze, K., and Viola, G., 2007, The analysis of quartz c-axis fabrics using a modified optical microscope: Journal of Microscopy, v. 227, p. 30-41.

Wing, B. A., Ferry, J. M., and Harrison, T. M., 2003, Prograde destruction and formation of monazite and allanite during contact and regional metamorphism of pelites: Petrology and geochronology: Contributions to Mineralogy and Petrology, v. 145, p. 228-250.

Wolfram, L. C., Weinberg, R. F., Hasalová, P., and Becchio, R., 2017, How melt segregation affects granite chemistry: Migmatites from the Sierra de Quilmes, NW Argentina: Journal of Petrology, v. 58, p. 2339-2364.

Wolfram, L. C., Weinberg, R. F., Nebel, O., Hamza, K., Hasalová, P., Míková, J., and Becchio, R., 2019, A 60-Myr record of continental back-arc differentiation through cyclic melting: Nature Geoscience, v. 12, p. 215-219.